# ADVANCES IN THE SUBCRITICAL, GAS-COOLED, FAST TRANSMUTATION REACTOR CONCEPT

RADIOACTIVE WASTE MANAGEMENT AND DISPOSAL

**KEYWORDS:** *subcritical reactor, transmutation reactor, fuel cycle*

W. M. STACEY,* K. A. BOAKYE, S. K. BRASHEAR, A. C. BRYSON, K. A. BURNS, E. J. BRUCH, S. A. CHANDLER, O. M. CHEN, S. S. CHIU, J.-P. FLOYD, C. J. FONG, S. P. HAMILTON, P. B. JOHNSON, S. M. JONES, M. KATO, B. A. MacLAREN, R. P. MANGER, B. L. MERIWETHER, C. MITRA, K. R. RIGGS, B. H. SHRADER, J. C. SCHULZ, C. M. SOMMER, T. S. SUMNER, J. S. WAGNER, J. B. WEATHERS, C. P. WELLS, F. H. WILLIS, Z. W. FRIIS, J. I. MARQUEZ-DANIAN, R. W. JOHNSON, C. DE OLIVEIRA, H. K. PARK, and D. W. TEDDER *Georgia Institute of Technology*
*Nuclear & Radiological Engineering Program, Atlanta, Georgia 30332-0425*

Received May 25, 2006
Accepted for Publication November 1, 2006

*The design concept for a subcritical, He-cooled, fast reactor, fueled with transuranics (TRUs) from spent nuclear fuel in coated TRISO particles and driven by a tokamak D-T fusion neutron source, is being developed at Georgia Institute of Technology. The basic concept has been developed in two previous papers. This paper reports (a) advances in the design concept intended to enable achievement of "deep-burn" of the TRUs and passive safety, (b) investigations of the possibility of reprocessing the TRISO TRU fuel and of extending the strength of the fusion neutron source, (c) more extensive analyses to confirm and improve the design with respect to the adequacy of the fuel and nuclear performance, heat removal, tritium self-sufficiency and shielding, (d) more extensive analyses to confirm that the International Tokamak Experimental Reactor divertor, magnet and heating/current drive systems can be adapted, and (e) fuel cycle analyses to further investigate the contribution that such a reactor could make to closing the nuclear fuel cycle.*

## I. INTRODUCTION

A concept for a subcritical, fast reactor that would be fueled with transuranics (TRUs) from spent nuclear fuel (SNF) is being developed at Georgia Institute of Technology (Georgia Tech). Previous conceptual design studies[1–5] and fuel cycle analyses[6,7] have established a preliminary design concept for an annular subcritical fast reactor surrounding a tokamak fusion neutron source. The original fusion transmutation of waste reactor (FTWR) studies,[1,2,5,6] for subcritical integral fast reactors fueled with pure TRU in a metal form and cooled with liquid lithium, were undertaken to examine the use of a tokamak fusion neutron source instead of an accelerator spallation neutron source with a variant of the sodium-cooled, metal-fuel fast reactor that was developed in the Advanced Fuel Cycle Initiative Studies. The two previous gas-cooled fast transmutation reactor (GCFTR) studies,[3–5] for gas-cooled fast reactors fueled with pure TRU in coated particle form and cooled with He, were undertaken to investigate the possibility of using the TRISO-coated fuel particle concept to achieve very deep TRU burnup with minimal reprocessing steps and to use a gas-cooled reactor with relatively low power density to achieve a design that was passively safe with respect to a loss-of-coolant accident (LOCA). These studies are summarized in Appendix A. Previous analysis[3,4] identified the requirement for emergency core coolant in order for the GCFTR to survive a LOCA. Thus, one of the major purposes of this follow-on

*E-mail: weston.stacey@nre.gatech.edu

design study was to reexamine the requirement for an emergency core cooling system (ECCS) and to develop the design concept for a passively activated accumulator ECCS (Sec. V).

The results of a follow-on fuel cycle analysis[7] indicate that a GCFTR with a 200-MW fusion neutron source could meet the >90% TRU burnup objective with repeated recycling (~15% TRU burnup per five-batch burn cycle) with reprocessing to remove fission products and replenish depleted TRU. The results of this study suggested that in order to achieve the objectives of deep burn of TRU without reprocessing, the design of the GCFTR should be changed to either (a) allow for a stronger neutron source to compensate a greater negative reactivity accumulation $[P_{fis} \sim k_{eff} P_{fus}/(1 - k_{eff})]$, (b) admix $^{238}$U with the TRU fuel to produce fresh TRU fuel in situ to offset the negative reactivity decrement of TRU depletion and fission product buildup, or both. The second option would be inconsistent with a purely deep-burn transmutation goal for GCFTR, but would be consistent with the somewhat broader goal of more effective utilization of the uranium mined for nuclear fuel (including extraction of energy from the TRU in SNF).

Investigations of these two options for achieving deep burnup without reprocessing are also major purposes of this follow-on design study. The practical upper limit on fusion power (neutron source strength) for a tokamak of the dimensions of the GCFTR-2 neutron source[3] (major radius 3.7 m, minor radius 1.1 m) operating within the International Tokamak Experimental Reactor (ITER) design database[8] was evaluated, in order to determine the allowable increase of fusion neutron source strength that is available to compensate the reactivity decrease due to fission product buildup and TRU depletion in the fuel kernels (Sec. VI). A redesign of the TRISO fuel particle to maximize the lifetime against fission product gas buildup was carried out, and the fuel pin clad radiation damage lifetime was evaluated for the previous reference Zircaloy and other clad materials (Sec. III). The consequences of admixing $^{238}$U with TRU within the TRISO fuel kernels to produce additional TRU to reduce the reactivity decrease due to fission product buildup and TRU depletion was also evaluated (Secs. IV and VII).

Since the follow-on fuel cycle analysis[7] indicated that, with repeated recycling with reprocessing, the previous GCFTR-2 design could achieve >90% TRU burnup with fusion neutron sources in the range $P_{fus} <$ 200 MW, another major purpose of this follow-on design study was to examine the feasibility of reprocessing the TRISO TRU fuel particles to remove fission products and add fresh TRU in refabricated TRISO fuel particles (Sec. III).

The core and neutron source designs and supporting analyses were extended in several respects. The neutron source heating and current drive system (H&CD) was defined (Sec. VI) and the requirement for port access through the shield and reactor into the plasma was taken into account. The core nuclear and thermal analyses, the shielding design and analysis, and the tritium production design and analysis were extended and refined (Secs. IV and V). The fusion neutron source engineering design analysis was extended to evaluate the heat removal capability of the ITER divertor adaptation when the coolant was changed from water to helium and to confirm the structural aspects of the adaptation of the ITER toroidal field (TF) coil (TFC) system (Sec. VI).

## II. DESIGN OVERVIEW

### II.A. Configuration, Dimensions, Materials, and Major Parameters

The GCFTR-2 reactor concept[3] was the starting point for the analyses described in this paper. This reactor is a subcritical, fast, helium-cooled reactor driven by a tokamak D-T fusion neutron source. The configuration, overall dimensions, magnetic field, and He coolant remained the same for the GCFTR-2 design, but an increase in the plasma current to achieve a more intense neutron source rate, changes of some fuel materials, definition of the heating and current drive and ECCS, and other changes were sufficient to designate a new design—the GCFTR-3 reactor. A three-dimensional (3-D) depiction of the GCFTR-3 is shown in Fig. 1. The annular reactor surrounds the fusion plasma neutron source on the outboard side, and both are surrounded by a combination reflector and lithium-oxide blanket for tritium production and then by a shield. (A divertor below the plasma and an accumulator for emergency core cooling above the core are not shown.)

The detailed radial dimensions are indicated (but not all shown) in Fig. 1. The inner radius of the reactor core is 485 cm, the core width is 112 cm (100-cm fuel region) and the core height is 300 cm. The tokamak fusion neutron annular plasma source is on the inboard side of the reactor, with a width of 216 cm and a height of 367 cm. A divertor is located on the bottom inboard side of the plasma chamber. The plasma chamber and divertor are scaled down from the ITER design.[8] A 3.5-cm-thick first wall of the plasma chamber separates the core and plasma regions. Both the plasma and the reactor core are surrounded by a blanket-shield which is 79.5 cm thick, which in turn is surrounded by a 6-cm-thick vacuum vessel. This entire annular configuration—reactor, plasma, blanket, shield, vacuum vessel—is contained within a ring of 16 "D-shaped" superconducting TFCs, each of radial thickness 43 cm and toroidal thickness 36 cm. The vacuum vessel abuts the TFCs on the inboard side. Just inside the torodial field magnets is the central solenoidal magnet of thickness 48 cm. The remaining "flux core" space inside the central solenoid (CS) has a radius of 88 cm.

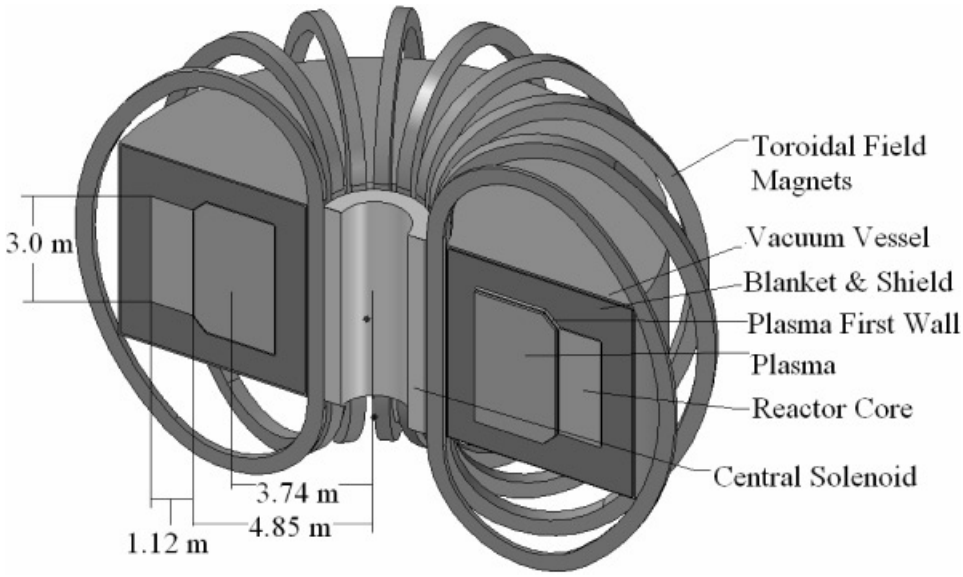


Fig. 1. Configuration of the GCFTR-3.

### II.B. Major Parameters and Materials

Table I gives the major parameters and materials used in the GCFTR-3. The parameters and materials were designed for a TRISO fuel particle that has a TRU-U-oxide kernel that is surrounded by SiC, WC, and ZrC layers, which are embedded in a SiC matrix. All structural materials are oxygen-dispersion-strengthened (ODS) martensitic steel.

### II.C. Component Radiation Damage Lifetime

Fuel lifetime against radiation damage is crucial for the achievement of the TRU burnup objectives of GCFTR-3. In the reprocessing option, in which deep burnup is achieved by repeated 8.2-yr, five-batch burns that each achieve 25% TRU burnup, the minimum requirement is survival of the fuel for a fast (>0.1 MeV) neutron fluence of $6.9 \times 10^{22}$ n/cm$^2$. In the nonreprocessing option, in which deep burnup is achieved in a single 33.9-yr, five-batch burn that achieves 94% TRU burnup, the requirement is survival of the fuel for a fast (>0.1 MeV) neutron fluence of $4.3 \times 10^{23}$ n/cm$^2$.

Unfortunately, there is little data for TRISO particles at deep burnup in a fast neutron spectrum. The Peachbottom Reactor irradiated TRISO particles with a fast fluence of $1.3 \times 10^{21}$ n/cm$^2$ at temperatures from 800 to 1350°C, with a failure rate of $1.4 \times 10^{-6}$ (Ref. 9). More recent results from development programs in the United States and Germany have achieved burnups as large as 80% and fast neutron fluences as large as $1.2 \times 10^{22}$ n/cm$^2$ with failure rates of $10^{-4}$ to $10^{-6}$ for the higher burnup US tests and $10^{-7}$ to $10^{-9}$ for the order 10% burnup German tests.[10] Achievement of the fluence lifetimes required for a deep-burn transmutation reactor like GCFTR-3 is a major challenge for TRISO fuel development.

The fuel cladding and fuel assembly structure lifetimes against radiation damage are also important considerations. The minimal requirement for the ODS clad is to survive the five-batch residence time of 8.2 yr for the reprocessing option, which corresponds to a fast neutron fluence of $6.9 \times 10^{22}$ n/cm$^2$. The maximum requirement for the ODS clad is to survive the single five-batch residence time of 32.9 yr for the nonreprocessing option, which corresponds to a fast neutron fluence of $4.3 \times 10^{23}$ n/cm$^2$. Lifetime of the ODS martensitic steel structure can only be estimated; using the values of 80 to 150 displacements per atom estimated for HT-9 (Ref. 11) corresponds to 1.5 to 3.0 $\times$ $10^{23}$ n/cm$^2$ fast neutron fluence.

The plasma chamber "first wall," which consists of 3 cm of ODS martensitic steel coated with 0.5 cm of Be, would receive a fast neutron fluence of $7.5 \times 10^{23}$ n/cm$^2$ over 30 effective full power years (EFPYs) of operation. Using the same estimate for the radiation damage lifetime of ferritic steel as above, this would require two to four first wall replacements.

The shield was designed to protect the superconducting magnets from radiation damage failure over a 30 EFPY lifetime.

The ITER divertor,[8] after which the GCFTR-3 divertor is modeled, is expected to require replacement eight times during ITER lifetime because of plasma erosion of the surface. The plasma flux to the divertor in ITER is a few times greater than in GCFTR-3, but the GCFTR-3 lifetime is several times longer than that of

TABLE I

Major Parameters and Materials of the GCFTR-3

| Parameters and Materials | Values |
|---|---|
| Reactor | |
| Annular dimensions (m) | $R_{in} = 4.85$, $R_{out} = 5.97$, $H = 3$ |
| Fuel/He/structure (vol%) | 60/30/10 |
| Fuel element | TRISO particles in SiC matrix, pins $d = 1.34$ cm |
| TRU-U coated particle diameter ($\mu$m) | 660 |
| TRU-U-oxide fuel packing factor (%) | 62 |
| TRU-U fuel mass (metric tons) | 74 |
| Maximum $k_{eff}$ (kg/s) | 0.95 |
| He mass flow, He temperature (°C) | $M = 3280$, $T_{\rm He}^{in}/T_{\rm He}^{out} = 280/494$ |
| Power density (MW/m$^3$), maximum $T_{fuel}$ (°C) | $q''' = 42.2$, $T_{fuel}^{\max} = 669$ |
| Clad/structural materials | ODS martensitic steel |
| Fission power [MW(thermal)] | 3000 |
| Blanket shield | |
| Shield materials | ODS steel, He, $B_4C$, HfC, Ir, WC, Cd |
| Tritium breeder | $Li_2O$ |
| Thickness (cm) | 79.5 |
| TBR | 1.1 |
| Plasma | |
| Plasma current (MA) | ≤8 to 10.0 |
| Fusion power (MW)/neutron source rate (s$^{-1}$) | (50 to 500)/(1.8e19 to 1.8e20 s$^{-1}$) |
| Fusion gain ($Q_p = P_{fus}/P_{plasma\ heating}$) | 3.2 to 5.1 |
| Superconducting magnets | |
| Field CS, TFC, on center of plasma (T) | 13.5, 11.8, 5.9 |
| Divertor | |
| Materials | W tiles on CuCrZr, He-cooled |
| Heat flux (MW/m$^2$) | ≤2.0 |
| First wall | |
| Materials | Be on ODS, He-cooled |
| Neutron wall load (14 MeV) (MW/m$^2$) | ≤1.8 |
| Heat flux (MW/m$^2$) | ≤0.4 |

ITER, so that tens of divertor replacements might be anticipated for GCFTR-3.

The radiation damage lifetime estimates are summarized in Table II.

## III. FUELS

### III.A. The Fuel Kernel and TRISO Particle

The TRISO fuel particle was selected over the BISO since the TRISO's additional layer provides more structural support. This reduces the actual fuel capacity within the reactor but provides a more stable particle, which is desirable from a lifetime standpoint.

With respect to Fig. 2, the particle consists of a center fuel kernel surrounded by a ZrC buffer and three supporting layers. The buffer absorbs fission gases and serves to stop recoil fission products. The innermost WC layer serves as a shield to protect the kernel from chlorine, which is used in the fabrication process in bonding the subsequent coatings. The SiC layer is the primary structural component, and the outer WC layer provides an extra layer of protection.

For survival in a fast reactor, it was necessary to modify the conventional TRISO particle, which was developed for thermal reactors. In thermal reactors, pyrolytic carbon has been used to form both the inner and outermost coatings after the buffer. Unfortunately, pyrolytic carbon contracts under irradiation at a rate proportional to neutron energy; therefore, the inner layer may contract too quickly in a fast flux and become unattached to the next layer. This results in cracking and failure of the particle.[13] WC has an ultimate tensile stress of 344 MPa and a high modulus of elasticity, which make it a possible replacement for pyrolytic carbon, which has a

TABLE II

Component Radiation Damage Lifetimes

| Component | GCFTR-3 Fast Neutron Fluence ($n/cm^2 > 0.1$ MeV) | LIMIT Fast Neutron Fluence ($n/cm^2 > 0.1$ MeV) |
|---|---|---|
| Reactor | | |
| Clad | | |
| 8.2 yr, 25% TRU burnup | $6.9 \times 10^{22}$ | 1.5 to $3.0 \times 10^{23}$ [a] ? |
| 32.9 yr, 94% TRU burnup | $4.3 \times 10^{23}$ | 1.5 to $3.0 \times 10^{23}$ [a] ? |
| TRISO fuel particle | | |
| 8.2 yr, 25% TRU burnup | $6.9 \times 10^{22}$ | ? |
| 32.9 yr, 94% TRU burnup | $4.3 \times 10^{23}$ | ? |
| Fusion neutron source | | |
| TFC $Nb_3Sn$ 30 EFPY | $1.6 \times 10^{18}$ | $1 \times 10^{19}$ [b] |
| TFC insulation 30 EFPY | $3.1 \times 10^{7}$ rad | $10^{9}$ to $10^{10}$ rad[b] |
| First-wall 30 EFPY | $7.5 \times 10^{23}$ | 1.5 to $3.0 \times 10^{23}$ [a] ? |
| Divertor | | Plasma erosion |

[a]Reference 11.
[b]Reference 12.

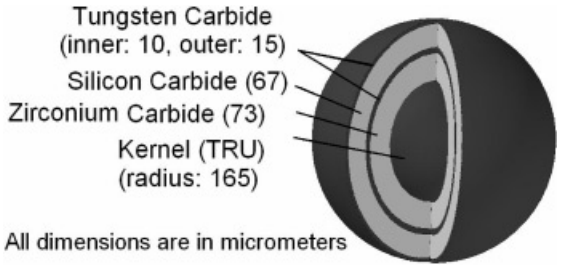


Fig. 2. TRISO particle.

lower ultimate tensile stress of approximately 160 MPa. The melting temperature of WC, 2780°C, is well above the peak temperature calculated for the LOCA scenario with a passively activated ECCS (Sec. V), which implies a significant margin between the WC melting temperature and any anticipated peak fuel temperature. The layer after the buffer consists of silicon carbide, which provides the primary structural support for the particle. Zirconium carbide with 50% porosity has been chosen for the buffer layer since a material with a high affinity to oxygen is needed[4] to control the buildup of oxygen-based gases.

The particles receive an intense amount of high-energy neutron radiation during their lifespan, which may cause swelling and cracking.[14] Extensive research on TRISO particles in both fast and thermal fluxes has been done, indicating that these failure mechanisms are of concern only when large temperature gradients in individual particles or particle irregularities outside of manufacturing specifications occur.[14,15] Because of the inability to obtain pertinent data regarding these failure mechanisms for the designed particle, only pressure buildup due to gaseous fission products inside the particle was examined quantitatively.

With a fuel consisting initially of 70% TRU-oxides and 30% $^{238}U$, ORIGEN-S (Ref. 16) predicted a 73% reduction of the amount of TRU in the kernel after 30 000 days. Predicted fission gas concentrations for up to 30 000 days operation were used to calculate the pressure within the particle and projected linearly to predict pressures at 90% burnup. Helium, krypton, iodine, xenon, and bromine gases were the main contributors to pressure buildup.[4] At the nominal maximum fuel centerline operating temperature of 942 K (Sec. V), it was assumed that the gases could be modeled as ideal. Because the silicon carbide layer is the dominant structural layer in the particle and has a radius <10% of the total kernel radius, the stress in the particle wall could be calculated using expressions for a thin-walled pressure vessel. The particle size was optimized using the assumptions above, and keeping the sum of the thicknesses of the buffer and SiC layers constant. A slight reduction was taken from the optimized buffer radius in order to preserve the assumption of a thin-walled pressure vessel. The inner layer, which serves as a chemical shield during the fabrication process, is bonded to the second layer, and because it provides little structural support, it is ignored in the initial optimization.[17] The kernel diameter was set to 330 $\mu$m to accommodate the core fuel density necessary for adequate neutron multiplication. The final layer dimensions and material properties are given in Table III.

Using these dimensions, the pressure in the buffer was calculated at various burnups. Pressure and stress in each layer are plotted versus burnup in Fig. 3. The interior pressure increased linearly to 44.4 MPa at 90% burnup,

TABLE III

TRISO Particle Dimensions and Properties

| | Thickness ($\mu$m) | Ultimate Tensile Stress (MPa) | Young's Modulus (GPa) | Poisson's Ratio | Density (g/cm$^3$) |
|---|---|---|---|---|---|
| Kernel (radius) | 165 | | | | |
| Buffer | 73 | | | | |
| Inner WC | 10 | 344 | 668 | 0.24 | 15.8 |
| SiC | 67 | 200[a] | 410 | 0.14 | 6.73 |
| Outer WC | 15 | 344 | 668 | 0.24 | 15.8 |

[a]Silicon carbide was noted by NIST as having $\sigma_{UTS} = 200$ MPa. Other values have been noted, but this takes the most conservative approach.

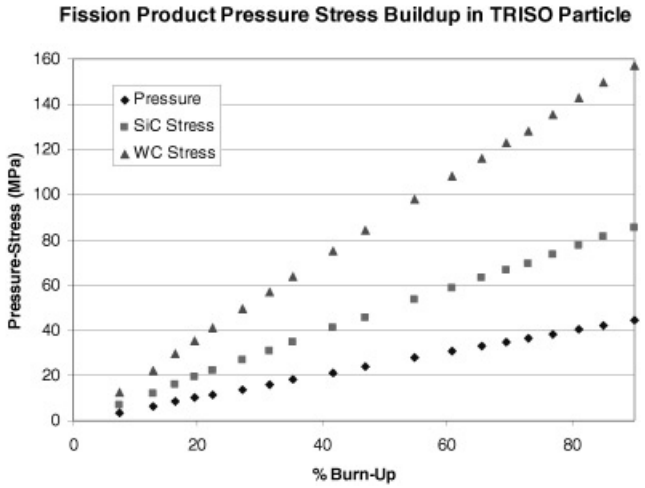


Fig. 3. Pressure and stress versus burnup.

and this pressure creates a stress of 85.4 MPa on the SiC layer.

The outer layer is not susceptible to failure due to gas pressure, but expansion of the silicon carbide layer is of concern. Calculations using Young's Modulus and Poisson's Ratio were used to determine the amount of stress in the outer layer due to interior expansion. At 90% burnup, the WC will have a stress of 157.4 MPa applied to its inner wall. Pressure and stress in each layer are plotted versus burnup in Fig. 3. Because of the large differences between the ultimate tensile strengths of the layer materials and the stresses expected to be placed on the layers, it is not anticipated that the particle will fail because of fission product gas pressure buildup at the nominal operating temperatures. For the same reason, the particle can withstand a temperature transient up to 1318 K, a reduction in ultimate tensile strength by 57%, or a decrease in either the buffer or SiC layer without the fission gas pressure at 90% burnup exceeding stress limits. Because SiC hardens with irradiation,[18] an additional measure of conservatism is inherent in these calculations.

Radiation damage remains an essential concern in determining the lifetime of the particle, but more research will be needed before the subject can be further explored. In addition to material changes and transmutation gas buildup due to $(n, p)$ and $(n, \alpha)$ reactions in all components due to neutron irradiation, shear stress between the coating layers of the particle may cause cracking which could lead to particle failure.[19] Kernel migration in the buffer and associated hot spots also require further work. It may be possible to change material of the buffer to decrease kernel shifting, so long as a material with an affinity for oxygen and porosity is used. Additionally, WC is a new material for this application, and additional research into it is needed.

### III.B. Cladding

The cladding for the GCFTR-2 design was Zircaloy-4 alloy.[3] A major problem with Zircaloy, however, is that it expands extensively in a fast neutron spectrum.[14] This would make fuel pin design very difficult, and therefore determination of a more promising clad material was an objective of this study. Two materials that were strongly considered for cladding for this reactor design were ODS martensitic steel and SiC, the properties of which are given in Table IV.

TABLE IV

Cladding Materials*

| | Operating Temperature (K) | Melting Temperature (K) | Main Disadvantage |
|---|---|---|---|
| Zircaloy-4 | <2118 | 2118 | Expands under fast flux; low melting point |
| SiC | 923 to 1223 | 3646 | Brittle |
| Ferritic/martensitic steel | 543 to 773 | 1400 to 1500 | Low melting point |
| ODS martensitic steel | 598 to 983 | 1400 to 1500 | Low melting point |

*Reference 23.

TABLE V

Compositions (%) of ODS and HT9*

| Alloy | 1DS | HT9 |
|---|---|---|
| Fe | Balance | Balance |
| Cr | 11.0 | 12.0 |
| W | 2.7 | 3 Mo |
| Ti | 0.5 | 0.5 |
| Ni | 0.1 | 0.1 |
| C | 0.1 | 0.2 |
| P | 0.005 | 0.01 |
| S | 0.001 | 0.005 |
| Free O | 0.11 | — |
| $Y_2O_3$ | 0.6 | n.a.[a] |

*Reference 26.
[a]n.a. = not applicable.

As shown in Table V, 1DS steel, a typical ODS, has a similar composition to HT-9, a typical ferritic/martensitic steel, but has differences due to the addition of $Y_2O_3$ particles. HT-9 has been widely used in fast reactors in the past because, unlike austentic steels, it has excellent swelling resistance. The ODS steel retains these excellent swelling resistance properties.[20] The small $Y_2O_3$ precipitates (<20 nm) present in ODS steel serve two major purposes. First, they stabilize the matrix by blocking mobile dislocations. Second, they act as a sink of radiation-induced point defects.[21] This allows the ODS steels to be more stable at higher operating temperatures while maintaining reasonably similar mechanical and thermal properties to HT-9.

There are several drawbacks to ODS steel. The melting temperature, 1400 to 1500 K, falls short of the clad temperature calculated in LOCA analyses of GCFTR without emergency core cooling (Sec. V). Early ODS steels had trouble with anisotropy in mechanical properties. However, recent developments in the heat treatment process have alleviated this problem.[22] The hardness of the material initially caused some complications in processing, but this problem has also been solved.[21] In addition, ODS steel has marginal oxidation resistance at high temperatures.[23]

SiC has several advantages that make it an excellent candidate for cladding in high-temperature fast reactors. It has an extremely high melting point (~3400 °C), very high strength [ultimate tensile strength (UTS) ~200 MPa], and low swelling (~1%) (Ref. 18). Brittleness is an issue with pure SiC, but fracture toughness of SiC fibers in a SiC matrix (25 MPa $m^{1/2}$) (Ref. 24) is nearly an order of magnitude higher than that of pure SiC (3.1 MPa $m^{1/2}$) (Ref. 25). Another issue that needs to be addressed in pure SiC is the thermal conductivity degeneration due to high temperature irradiation. However, certain SiC composites show a lesser decrease in thermal conductivity than pure SiC (Ref. 24).

An ODS martensitic steel was chosen for the reference cladding material. SiC was not chosen largely because of the lack of published data on its current use in fast reactors.

### III.C. Fuel Fabrication

The TRISO fuel kernels will be fabricated using a sol-gel (solution-gelation) process. The TRUs coming from the UREX/TRUEX processes will be in a nitrate form. In order to change the nitrate into a hydroxide and ultimately an oxide, the following chemical reaction occurs in the mixer in Fig. 4:

$$\mathrm{TRU(NO_3)}_X + X\mathrm{NH_4OH} \rightarrow \mathrm{TRU(OH)}_X(\downarrow) + X\mathrm{NH_4NO_3} \ ,$$

where $X$ depends on the valence state of the particular element being reacted. The sol is obtained by first mixing the TRU nitrate [$\mathrm{TRU(NO_3)}$] with ammonium hydroxide ($\mathrm{NH_4OH}$) and the resulting TRU hydroxide [$\mathrm{TRU(OH)}$] precipitates out of solution. The ammonium nitrate is removed by stirring the solution and washing with water. Then, nitric acid ($\mathrm{HNO_3}$) is added to the TRU hydroxide precipitate to form the final sol. In order to avoid the use of a gelation agent, the nitric acid/TRU ratio must be 0.6 or higher. The sol is then heated to 70°C for about 3 h (Ref. 27), and a surfactant is added in order to keep particles from sticking together.[28]

The gelation process takes place by forcing the sol through a very small needle into a liquid atmosphere of 2-ethyl-hexanol (2-EHOH). Surface tension forms the sol into droplets which are proportional in size to the diameter of the needle. Gravity forces the droplets downward against a countercurrent of 2-EHOH. 2-EHOH extracts the remaining water from the droplets left over

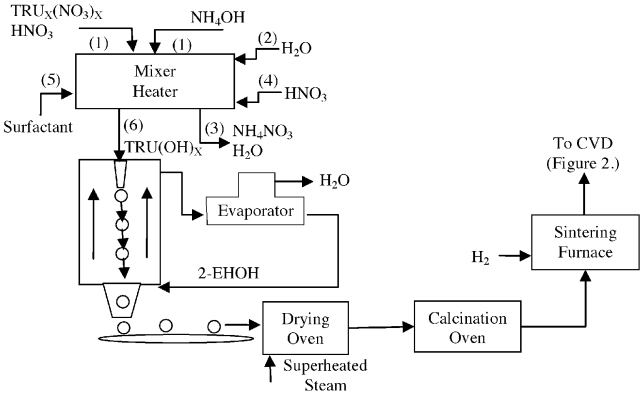


Fig. 4. Kernel fabrication.

from the sol stage. The 2-EHOH is contained in a separate loop and is run through an evaporator to remove the excess water and recycle the 2-EHOH. The kernel droplets are released from a nozzle one at a time onto a conveyor belt where the 2-EHOH is drained off.[27]

The droplets are then dried in an atmosphere with superheated steam at 250°C for 10 min. Drying in an atmosphere of superheated steam allows for a more even drying from the inside of the kernel to the outside, which prevents cracking.[28] The kernels are then sent through a calcination oven at 300°C in an air atmosphere. Lastly, the kernels are sintered in a reduction furnace in an atmosphere of $H_2$ at a temperature of 1600°C. This is where the fuel form can further be controlled. The $H_2$ combines with the oxygen in the fuel to form water. So, the more $H_2$ present in the atmosphere, the lower the oxygen content of the final fuel kernel.[10]

The TRISO particle's fabrication process is depicted in Fig. 5. The layers will be fabricated using chemical vapor deposition (CVD). This will be a continuous process, similar to the German process,[10] rather than a batch process with a sintering step as previously used in the United States.[10] The continuous process and the higher coating rates are felt to contribute to a more resilient fuel particle.[10] CVD works on the principle of a temperature difference between the particle and the surrounding vapor, which consists of a mixture of argon and the gaseous material to be deposited. The particle, which is constantly rolling through the deposition oven, is at a relatively cooler temperature than the surrounding vapor. The vapor essentially condenses evenly on the particle, thereby forming that particular layer of the TRISO particle. Deposition rates typically vary between 4 to 10 $\mu$m/min, and the length of the deposition oven is dependent on how thick the desired layer must be and the deposition rate. There are also aging ovens between each deposition stage in order to allow for the layer to cure and the particle to cool back down to a suitable temperature.

Once the TRISO particles are ready, fuel pellets will be fabricated. These are made using chemical vapor infiltration[29] (CVI). These cylindrical pellets consist of TRISO particles embedded in a SiC matrix. CVI is only

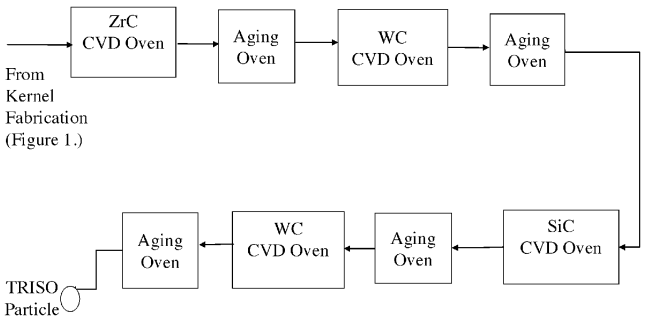


Fig. 5. TRISO particle layer fabrication.

TABLE VI

Fuel Pin Parameters

| | |
|---|---|
| Flat-to-flat distance (cm) | 36.625 |
| Side length (cm) | 21.146 |
| Assembly height (cm) | 300 |
| Pin diameter w/clad (cm) | 1.526 |
| Pins/assembly | 384 |
| Assemblies/core | 245 |
| Total pins in core | 94 080 |

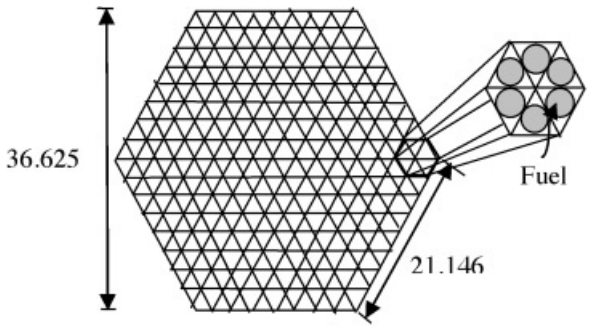


Fig. 6. Fuel assembly cross section.

useful for short distances because of potential blocking of the tubes as SiC travels through the packed TRISO particles. This limits the pellet to only 5.08 cm (2 in.) in length. A maximum packing factor for this geometry of 62% could theoretically be achieved. However, a realistic packing factor for this geometry is 50 to 60% (Ref. 3). These fuel pins are then stacked end-on-end and surrounded with a steel cladding and sealed on both ends.

The fuel assembly is hexagonal with a triangular grid (Fig. 6 and Table VI). There will also be a spacer grid midway up the assembly. The total number of assemblies in the core is 245. There are no half-assemblies due to the complication of fabricating half-assemblies.

The use of carbide fuels needs to be closely examined. Carbides may be superior to oxides because of the lower vapor pressure of AmC than $AmO_X$. Also, if carbides were used, there may be less of a need for the large ZrC oxygen-getter layer of the particle thereby allowing for a larger fuel kernel and a higher fuel volume percent.

The use of a melt-casted metallic fuel pellet instead of TRISO particles[30] should be examined.

### III.D. Reprocessing

As discussed above, the designed fuel particle is expected to withstand fission product pressure buildup to high burnup, but radiation damage or the reactivity decrement associated with high burnup may make it necessary to remove the particles before 90% actinide burnup

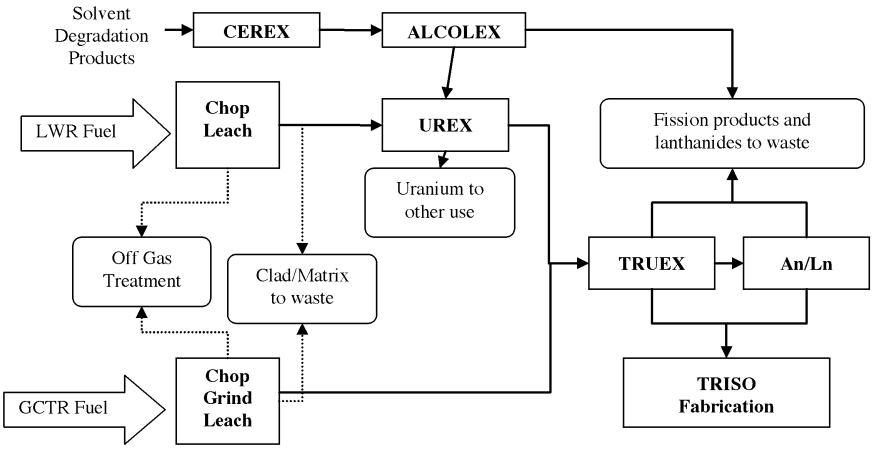


Fig. 7. Proposed combined LWR/GCFTR fuel recycle processes.

has been achieved. Thus, we investigated a possible reprocessing scheme which integrates the GCFTR fuel recycle with a light water reactor (LWR) fuel reprocessing facility. The UREX/TRUEX series has been selected over the DIDPA process which was previously presented[3] due to the buildup of degradation products in the DIDPA organic solvent limiting recycles. The CEREX (Ref. 31) and ALCOLEX (Ref. 32) processes have been proven to be efficient in removing degradation products from the tributyl phosphate utilized as an organic solvent in UREX and TRUEX, allowing for sufficient recycle of the organic solvent. The modeled process is shown in Fig. 7.

All of the processes shown have been investigated and described in the literature,[33,34] with the exception of the grinding of TRISO particles. Only the LWR Chop Leach and LWR UREX processes are necessarily commercial scale; the other processes are much smaller (hot cell) since actinides make up only ~1% of the spent fuel from the LWR and residence time in the GCFTR is significantly longer than that of a typical LWR. The proposed facility will utilize traditional "chop leach" head-end processes to separate the LWR fuel from the cladding. The separated LWR fuel will go into UREX to separate uranium for reuse or disposal; the UREX process has been demonstrated to achieve uranium extraction of >99.99% on a laboratory scale.[35–37]

To accommodate the TRISO particle, the headend process for the GCFTR fuel includes a grinding step to completely crush the particle into pieces no larger than 250 $\mu$m to ensure complete fuel kernel exposure for reprocessing. The two streams will be combined in the TRUEX step for recovery of TRUs (some of the remaining 0.01% uranium will coextract). Following TRUEX, the extracted material will go through a final An/Ln separations process to remove remaining lanthanides from the TRU before going on to fuel fabrication. The TRUEX and An/Ln separations have been tested with greater than 99.8% recovery of TRU from high level liquid waste and fuel.[33,34]

All of the steps associated with the GCFTR fuel require hot cell shielding for safety due to the increased radiological hazard presented by the buildup of certain isotopes. While the changing nature of the fuel presents a challenge for operations, it also limits proliferation risk as the material is not considered weapons viable after a few recycles.

Further research into reprocessing is necessary to determine critical geometry, actual chemical material balance, and cost data. While reprocessing of TRISO particles is feasible, it is difficult because of the need for destruction of the TRISO particle and because of significant waste material collection, and a less permanent fuel form is suggested if reprocessing is required.

## IV. NUCLEAR

### IV.A. Nuclear Calculation Codes and Models

Horizontal and vertical cross-section views of GCFTR-3 are given in Figs. 8 and 9 (refer to Tables I and VII for compositions.) To model the core, the multidimensional multigroup spherical harmonics code EVENT (Ref. 38) and the 3-D continuous energy Monte Carlo codes MCNP (Ref. 39) and KENO (Ref. 40) were used. Both the MCNP and KENO models used the ENDF/B-V and ENDF/B-VI cross-section libraries. Two separate two-dimensional (2-D) (*r-z* and *x-y*) EVENT models were used. Three-dimensional EVENT and MCNP models that exactly represented the reactor core dimensions and compositions, including the two 20-deg core sectors at 180 deg from each other devoted to H&CD ports (Sec. VI), were also used. The 2-D EVENT *r-z* model was used to represent the effect of axial leakage, and the *x-y* EVENT model was used to represent

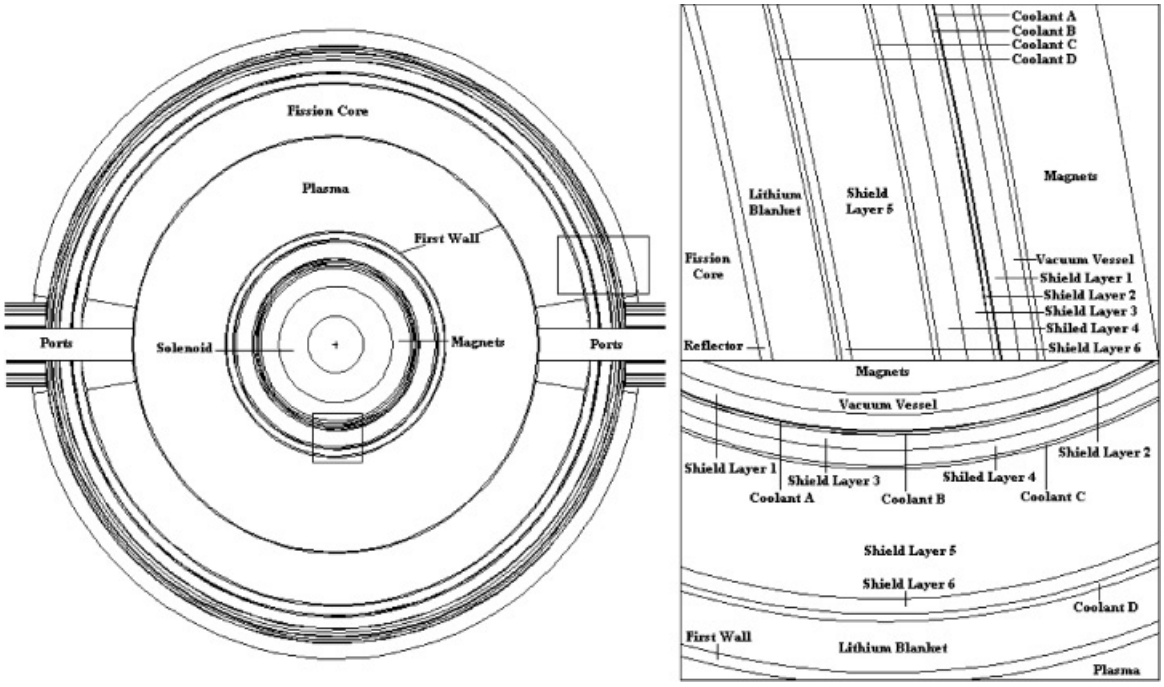


Fig. 8. Horizontal cross-sectional view of the GCFTR-3 reactor.

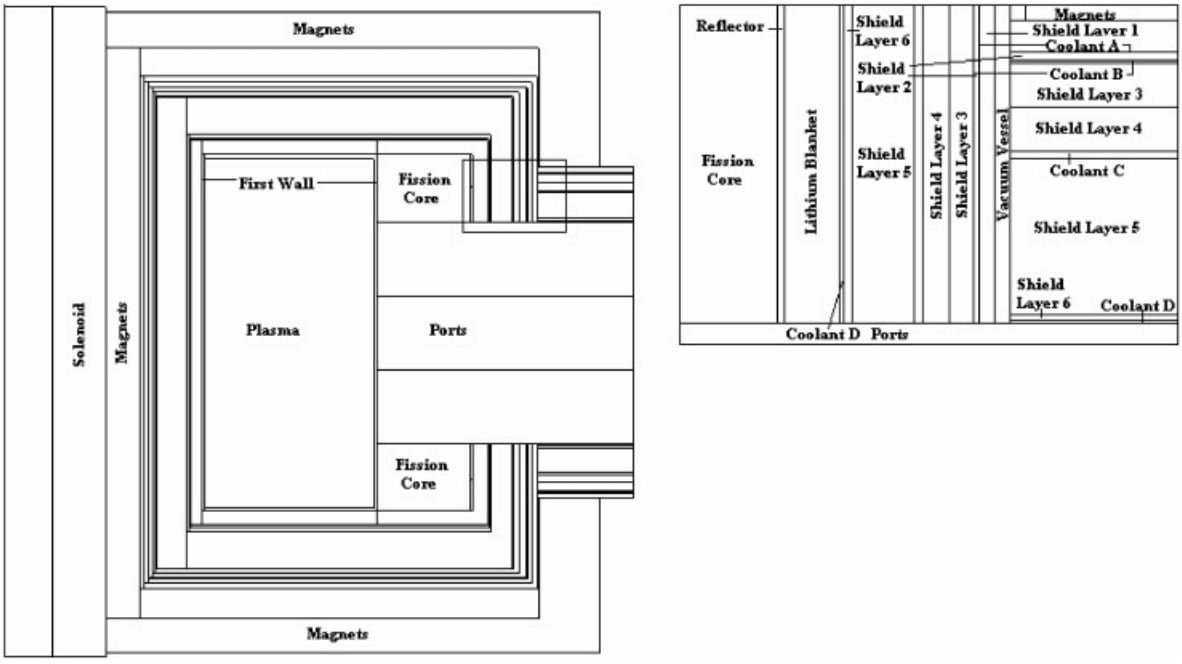


Fig. 9. Vertical cross-sectional views of the GCFTR-3 reactor.

the effect of these 20-deg sectors. The EVENT models used 34 energy groups (14 MeV to thermal) and a first-order ($P_1$) spherical harmonic approximation for all calculations (except the shielding calculation). (The $P_1$ approximation introduces some error near the plasma source in the highest energy groups where the anisotropic scattering of the 14.1 MeV fusion neutrons is important, but otherwise should be adequate for the

TABLE VII

Shield Layers and Compositions

| Layer | Material | Thickness (cm) | Density ($g/cm^3$) |
|---|---|---|---|
| Reflector | ODS steel | 3.5 | 7.9 |
| 1 | Iridium (Ir) | 4.75 | 22.4 |
| Cool A | Helium (He) | 0.25 | 0.1785 |
| 2 | Cadmium (Cd) | 0.95 | 8.65 |
| Cool B | Helium (He) | 0.05 | 0.1785 |
| 3 | Boron-carbide ($B_4C$) | 4.5 | 2.5 |
| 4 | Tungsten-carbide (WC) | 4.5 | 15.7 |
| Cool C | Helium (He) | 1.0 | 0.1785 |
| 5 | Hafnium-carbide (HfC) | 38.25 | 12.76 |
| 6 | Tungsten-carbide (WC) | 4.5 | 15.7 |
| Cool D | Helium (He) | 2.25 | 0.1785 |

purposes of this paper.) Cross sections were acquired from an ISOTXS format library that had been generated from a FIDO file by a run of the TRANSX (NJOY) program.[41]

The composition of the TRU fuel is given in Appendix B.

### IV.B. Multiplication Constant

#### *IV.B.1. Range of Multiplication Constant*

The primary goal of the GCFTR-3 is to achieve a deep burn of the TRU actinides, while keeping $k_{eff}$ below 0.95 yet above the minimum value that can be compensated by increasing the power of the fusion neutron source. This minimum value of $k_{\min}$ can be roughly estimated by recalling that the fission power, which is roughly proportional to the total neutron population $N$ in a subcritical reactor, scales[42] as $P_{fis} = \upsilon N \Sigma_f = \upsilon \Sigma_f (\ell S/(1-k)) \sim kP_{fus}/(1-k)$, where $\ell = (\upsilon \Sigma_a)^{-1} \approx (\upsilon \Sigma_f (\nu/k))^{-1}$ is the neutron lifetime and $S$ is the fusion neutron source in the reactor. Making use of the calculated result that ~50 MW of fusion power was needed for GCFTR-2 to sustain a fission power of 3000 MW with a multiplication factor of 0.95 (Refs. 3 and 4) indicates that a fission power of 3000 MW can be maintained as low as $k_{\min} \approx 0.8$ by a fusion neutron source rate corresponding to $P_{fus} \simeq$ 200 MW. As shown in Sec. VI, it is possible to increase the fusion neutron source power to ~500 MW by increasing the current by ~20% if the physics database is extrapolated somewhat beyond the present limits. This would result in an even lower tolerable $k_{\min} \approx 0.5$ for operation at 3000-MW fission power. It should be noted that $k_{\min}$ is the subcritical neutron multiplication factor, which is different than the eigenvalue $k_{eff}$, but using $k_{\min} \approx k_{eff}$ provides useful guidance.

In order to gain some insight into the effect of fuel depletion on the range of the multiplication constant, a series of calculations was made for the pure TRU fuel. In these calculations, the fuel was uniformly distributed throughout the core, was not shuffled, and was uniformly depleted at 3000 MW(thermal), over 600-day intervals, using ORIGEN-S (Ref. 16). The multiplication constant was calculated for the fresh fuel and after each 600-day depletion interval, yielding a depletion reactivity decrement $\Delta k/k \approx -0.25$ at 3000 days of uniform depletion. As discussed in Sec. VII, the fuel will be burned five times, in different annular locations, so that in the steady-state fuel cycle the core will contain in any burn cycle fresh fuel, once-burned fuel, twice-burned fuel, thrice-burned fuel, and fuel that is burned four times.

#### *IV.B.2. Effect of H&CD Ports on Multiplication Constant*

One major change in the GCFTR-3 core from the original GCFTR design[3,4] is that 20-deg sectors have been removed from opposing sides of the annular reactor to make room for access ports for bringing H&CD power into the plasma, as shown in Fig. 8. These sectors are 20-deg (in the toroidal direction) wedges with respect to the central vertical axis removed from the annular reactor core, shield, and the first wall outboard of the plasma region.

Calculations of the annular core with no sectors removed and with two 20-deg sectors removed were made using the EVENT $x$-$y$ model to determine the effect of H&CD sector size on $k_{eff}$. The change in $k_{eff}$ from a fully annular core to one with 20-deg sectors removed 180 deg apart was ~1%, which established that removal of 20-deg sectors does not have a large reactivity effect.

### IV.C. Tritium Breeding Blanket

A tritium breeding blanket (TBB) containing lithium-oxide is shown in Figs. 8, and 9. This blanket surrounds the core and the plasma fusion source to breed tritium in order to fuel the plasma. (Tritium can be produced by fast- or low-energy neutrons via the exothermic reaction with $^6$Li, which constitutes 7.5% of natural Li, $n + {}^6\text{Li} \rightarrow T + {}^4\text{He}$, and by high-energy neutrons in the endothermic reaction with $^7$Li, which constitutes the remainder, $n + {}^7\text{Li} \rightarrow T + {}^4\text{He} + n'$.) To maximize the amount of tritium produced, a series of calculations was performed using ORIGEN-S in addition to iterative calculations to determine the optimal configuration of different $^6$Li and $^7$Li concentrations. The resulting composition of the $Li_2O$ blanket varies in enrichment from 30 to 90% $^6$Li. While the fraction of tritium produced from the $^6$Li reaction varies with position, overall it is about 10%. This configuration is shown in Fig. 10.

The power of the fusion source will vary from ~50 MW up to at most 500 MW. It is assumed that the

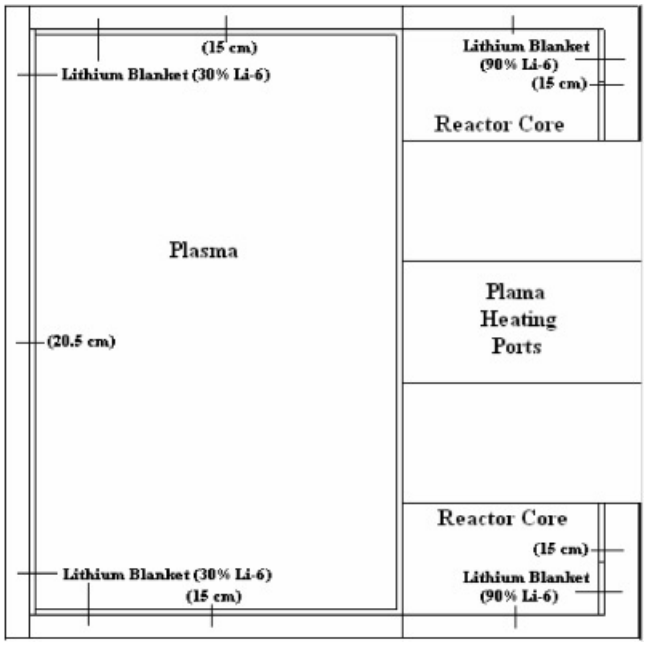


Fig. 10. Lithium-oxide blanket location and enrichment.

variation in source rate will be linear to compensate the linear drop in $k_{eff}$. The tritium breeding ratio (TBR = T produced/T consumed), which is the time-averaged value of the ratio of the tritium produced in the lithium blanket divided by the tritium consumed in the plasma, is a conventional measure of the capability for tritium self-sufficiency.

Tritium is removed from the $Li_2O$ by a helium purging system, then processed to separate it from the helium and other impurities present and stored to await injection into the plasma. It is assumed that the GCFTR will operate in burn cycles of 600 days with a shutdown of two weeks between cycles for fuel shuffling. There must be enough excess tritium at the end of a cycle to allow for a two-week decay and then to provide for at least a week of fusion operations in the next cycle until the online tritium gas purging and tritium processing system can begin providing fresh tritium. We estimate that TBR = 1.1 is needed to produce adequate tritium for self-sufficiency, allowing for decay, tritium loss, and purging loss. Using the EVENT *x-y* model, the neutron flux in each of the lithium regions was determined. Knowing the volume of each region and the incident flux, tritium production was simulated in ORIGEN-S for short intervals (1 day) to minimize the effects of tritium decay. For the GCFTR, a TBR of 1.08 was determined.

Tritium accumulation calculations were performed in order to determine whether the amount of tritium produced during operation is enough for the plasma to be self-sufficient. The total mass of the lithium blanket is $2.24 \times 10^5$ kg, and the total volume of the lithium blanket is $7.07 \times 10^7$ cm$^3$. Calculations used the flux distributions from the EVENT *r-z* model in ORIGEN-S to irradiate and decay the lithium in the blanket.

The amount of tritium that must be produced over a burn cycle for self-sufficiency is the amount required to replace the tritium burned over that burn cycle and to provide for one week of operation after restart, allowing for a 60-day decay between shutdown and restart of the next cycle. For the 600-day burn cycle, this requirement is for the production of 63.8 kg over the cycle. The calculations described above predict the production of 64.1 kg over the cycle, from which it may be concluded that the GCFTR-3 is tritium self-sufficient.

Lithium oxide ($Li_2O$) was chosen as the form for the blankets due to its high atomic density compared to other forms of lithium ($Li_2TiO_3$, $Li_2ZrO_3$, etc.). Online extraction of tritium from $Li_2O$ requires operation between 400 and 800°C. Below 400°C the rate of tritium diffusion out of the individual grains of $Li_2O$ is too slow, and above 800°C the particles swell and seal off porous channels through which the tritium must percolate to reach the helium purging channels.[43]

### IV.D. Power Distribution

The power distribution of the fission core was calculated with the EVENT *x-y* model. The total integrated power over the annular reactor core is approximately 3000 MW(thermal). This includes only the power generated in the fission core.

Figure 11 shows the normalized radial flux profile over the five core regions for a core with uniform fuel distribution at the beginning and end of a 600-day cycle. The regions are concentric equal-volume annuli extending from the inboard region 1 adjacent to the plasma neutron source to the outboard region 5 adjacent to the TBB and shield. The distribution is almost symmetric at beginning of cycle (BOC) when the fusion neutron source (located at left boundary) is small, but the effect of the

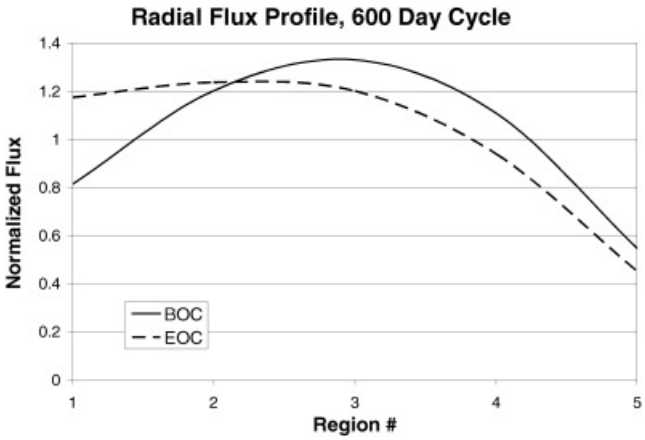


Fig. 11. Radial flux profile over five core regions.

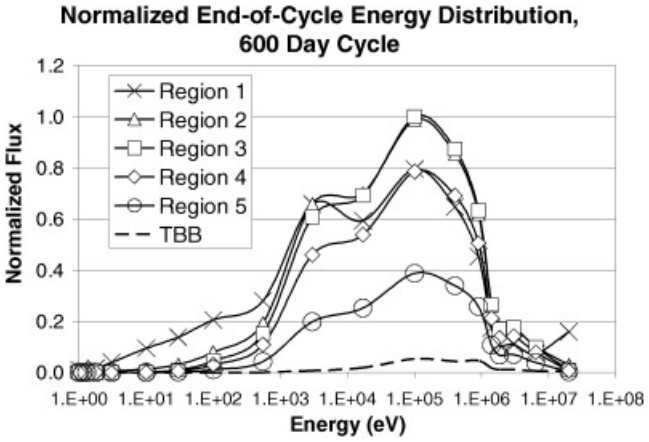


Fig. 12. Neutron spectra in fission core regions and lithium blanket.

increased neutron source at the end of cycle (EOC) is apparent.

### IV.E. Neutron Energy Spectrum

Figure 12 displays the neutron energy distribution in the five regions of the fission core and in the TBB surrounding the core. The neutrons in and surrounding the fission core are fast with essentially no thermal energies present. The neutrons leaving the fusion source are approximately 14 MeV, however they are moderated by the material surrounding the plasma chamber. The spectrum in the first core region next to the neutron source is similar to that for regions further away from the source—a broad spectrum with a mean energy of approximately 1 MeV—except for a small 14-MeV tail. In the TBB there is a prominent dip in the energy distribution slightly below 1 MeV due to resonance absorption due to $^{7}$Li.

### IV.F. Safety

#### *IV.F.1. Doppler Temperature Coefficient of Reactivity*

Doppler feedback is important for the inherently safe operation of the GCFTR-3. Calculations made using KENO found that the core had a temperature coefficient of $-0.9065 \pm 0.112$ pcm/K for pure TRU fuel. A reduction of $1\sigma$ in the temperature coefficient would yield a value of $-0.7945$ pcm/K, which would be considered the most conservative KENO estimate. This calculation was repeated with the EVENT *r-z* model and produced $-0.5885$ pcm/K.

The Doppler coefficient increased to $-1.2775$ pcm/K with the addition of 40% $^{238}$U in the fuel, as shown in Fig. 13. These calculations were made using KENO by varying the temperature in incremental steps from 800 to 1100°C for each fuel material composition in the core.

#### *IV.F.2. Reactivity Worth of Core Voiding*

In the event of a complete LOCA, the entire inventory of the helium coolant would be voided from the core. (A detailed analysis of the LOCA is provided in Sec. V.) To quantify the reactivity insertion due to a complete helium blowdown, calculations were made using the EVENT *x-y* model. The results of this calculation showed a positive reactivity insertion of 119 pcm for complete loss of He from the core.

#### *IV.F.3. Lithium Injection Module*

Another aspect of inherent safety that was studied is the use of $^{6}$Li as a shutdown mechanism, in the unlikely event that a supercritical condition occurred. Calculations were performed to obtain the amount of lithium that would be required to add ~5 dollars of negative reactivity into the core. The EVENT *x-y* model was used with various amounts of $^{6}$Li and $^{7}$Li, which were added to quantify their effects and compare the two isotopes. Using $^{6}$Li produced far better results than $^{7}$Li. A comparison of the cross sections of $^{6}$Li and $^{7}$Li showed that the absorption in the fast energies was approximately the same. The model determined that $5 \times 10^{19}$ atoms/cm$^{3}$ of $^{6}$Li would be required to introduce 5 dollars of negative reactivity. Considering the total volume of the reactor, this is ~600 g of lithium enriched to 95% $^{6}$Li.

Considering the concept of a lithium injection module[44] (LIM), after the temperature reaches a certain threshold the lithium would be released into the core. The LIM consists of a chamber located directly above the core in which the lithium is stored beyond a seal. The chamber is pressurized with gas that effectively pushes the lithium into the core after the seals have been broken.

At present there is no indication that a LIM will be needed for the GCFTR, which is intended to operate at all times with $k_{eff} \leq 0.95$. Further dynamic simulations of off-normal conditions are required for this determination.

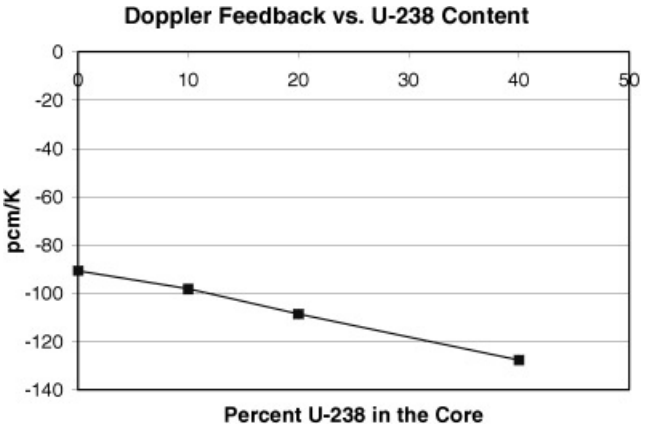


Fig. 13. Doppler feedback versus $^{238}$U content.

### IV.G. Shield

The primary purpose of the shield is to protect the superconducting TFC magnets from radiation damage. The shield also reduces radiation levels to an acceptable rate for other components. The maximum allowable dose rate[3,4] limit to the superconducting magnet insulators over a 40-yr period at 75% availability is $10^9$ to $10^{10}$ rads, depending on the insulator, the lower of which equates to 7.922 rads/s. The maximum allowable[3,4] fast neutron (>0.1 MeV) fluence to the superconductor is $10^{19}$ n/cm$^2$. The shield was modeled using MCNP with a volumetric neutron source representing the fusion plasma. The fusion neutron source was modeled as a uniform volumetric source that had a Gaussian distribution in energy around 14 MeV. Calculation of the flux was based on an average surface tally flux approximation. A surface tally counts the number of neutrons that hit a defined surface, giving a total tally of the flux (or neutrons per cm$^2$ per second) over that surface. To simplify the core, the fuel was modeled as a homogeneous mixture throughout each of the five equal-volume annular core regions.

The decision to remove two 20-deg sectors from the reactor and surrounding shield imposed a demanding constraint on the design of the shield. Extra shielding is required to reduce leakage from these H&CD ports. Shielding around the sectors was composed of the same materials and thicknesses as the main shield.

Four annular regions of different shielding materials were used for the GCFTR-3 design. The specific composition and density of each layer is given in Table VII. This shield surrounds the lithium-oxide blanket region.

Iridium, hafnium carbide, tungsten carbide, and boron carbide were chosen as shielding materials to thermalize and then absorb fast neutrons and gammas, while the cadmium layer was selected primarily to absorb neutrons. In addition, the entire shield was modeled to operate between 400 to 800°C.

Allowing for a maximum operating power level of 500 MW for the fusion neutron source, it is calculated, from MCNP, that the limiting fast neutron fluence to the superconductor and radiation dose to the insulator will not be exceeded, hence that the magnets will remain functional for their anticipated lifetime of 40 yr at 75% availability and that the nuclear heating of the magnets will be modest, as indicated in Table VIII. The main shielding layer, $B_4C$, will show a substantial depletion at this point resulting in an increase of the neutron flux at the magnets.

Helium coolant channels were sandwiched between each of the four layers of the shielding materials. The use of xenon coolant instead of helium coolant to enhance the absorption of thermal neutrons was considered. A comparative analysis determined that despite the significantly larger thermal cross section of xenon, there was only negligible difference in the performance of the shield because of the small number of thermal neutrons. After considering the heat removal capabilities of the two coolants, helium was chosen as the preferred coolant.

## V. THERMAL ANALYSIS

### V.A. Core Thermal Analysis

The fuel pin design was modeled after a standard pressurized water reactor pin, which consists of three layers. The inner material is composed of TRISO particles bound by a silicon carbide matrix into a cylindrical pin 0.6 cm in radius, as was described in Sec. III. A 0.01-cm helium gas-filled gap comprises the second layer of the fuel pin to account for thermal expansion. The final layer consists of a 0.06-cm ODS martensitic steel (which is represented by the thermal properties of HT-9 steel) cladding.

The reactor operates at a distributed power of 3000 MW(thermal), with an average volumetric heat generation rate of $q''' = 42.2$ MW/m$^3$. The thermal analysis performed on the fuel pin followed the form of a thermal circuit.[45] Values used in the circuit are presented in Table IX.

TABLE VIII

Shielding Performance

| Parameter | Limiting Dose[a] | MCNP Result | Time to End of Life (yr) |
|---|---|---|---|
| 40-yr fast neutron fluence to superconducting magnets at 75% availability | $10^{19}$ n/cm$^2$ | $1.57 \times 10^{18}$ n/cm$^2$ | >40 |
| 40-yr radiation dose to magnet insulators at 75% availability | $10^9$ to $10^{10}$ rads[b] | $3.06 \times 10^7$ rad | >40 |
| Nuclear heating in the magnets | | 34.5 kW | |
| Power for cooling toroidal magnets | | 3.9 MW | |

[a]References 3 and 4.
[b]Epoxy/ceramic.

TABLE IX

Fuel Pin Thermal Conductivities

| Pin Component | Thermal Conductivity (W/m-°C) |
|---|---|
| Silicon carbide | 120 |
| TRISO kernel | 27.6 |
| Zirconium carbide | 18.94 |
| Tungsten carbide | 84.02 |
| TRISO particle (homogenized) | 47.8 |
| Fuel pellet (homogenized) | 55.14 |
| HT-9 steel | 29 |
| Helium gap | 0.26 |

The value for the fuel pellet thermal conductivity was obtained by homogenizing the TRISO particle thermal conductivity with the silicon carbide matrix thermal conductivity based upon the mass percents of the materials. The gap coefficient was obtained from a previous study.[3] Using 33% of the melting point of the HT-9 steel cladding (445°C) as a limiting factor, the heat transfer coefficient for the helium coolant was found via the thermal circuit to be 4323 W/m$^2$-°C.

Applying the thermal circuit method, a distribution of bulk temperatures was calculated. The results are presented in Fig. 14. The lowest melting point of the materials comprising the fuel pin is the clad, which is 1327°C. Any effect of neutron irradiation on the thermal conductivity has not been taken into account.

The required mass flow rate of the helium coolant was found to be 3280 kg/s to keep the clad temperature at 33% of the melting temperature. A pumping power of 0.172 MW per assembly, or 42 MW for the reactor (245 assemblies), is required to pump the helium.

### V.B. Secondary Power Conversion System

A secondary electrical system is needed to convert the heat to useful electrical work. We adopt the system developed for GCFTR-2 (Ref. 3). Since helium is the coolant for the reactor, a typical Brayton cycle[46] that utilizes the He directly will be used. In order to realistically utilize the 3000 MW(thermal) that is being produced in the core, a total of four Brayton cycles will be used, one for each 90-deg segment of the reactor. Therefore, each Brayton cycle corresponds to 750 MW(thermal). Figure 15 shows one of the Brayton cycles and Table X identifies the properties at each section of the thermodynamic cycle.

The total electric power that is extracted from the 750 MW cycle is 255 MW(electric) corresponding to a thermal efficiency of 34%. The total electrical power for the entire reactor is 1020 MW(electric). However, in order to calculate the net amount of electrical power, the operating power requirements must be taken into consideration. These losses include power for all of the magnets involved in confinement (~30 MW), the H&CD systems for the plasma[5] (90 MW), and the coolant pumping power for both the core and the divertor (~200 MW). After taking into account all of the power used to operate the reactor, the net electrical power for the entire system is 700 MW(electric). The electrical power amplification factor ($Q_e$) is calculated as the total electrical power divided by the net operating power requirements, and this equals 3.19.

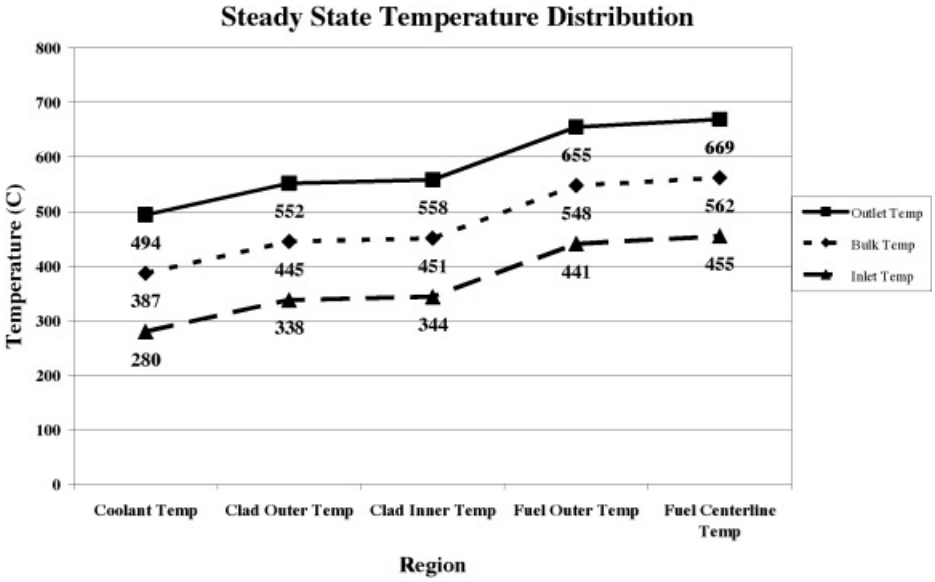


Fig. 14. Fuel pin temperature distribution.

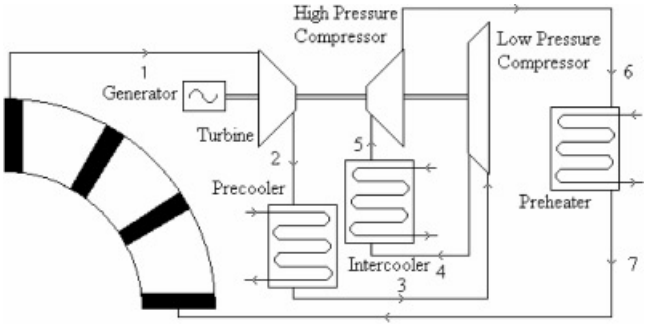


Fig. 15. Secondary electrical system diagram (Brayton cycle).

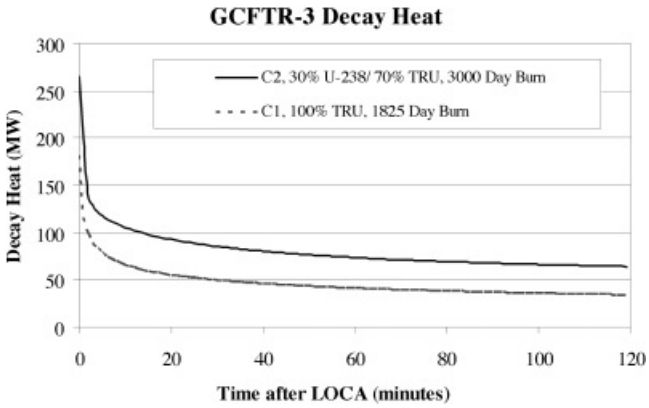


Fig. 16. Decay heat.

TABLE X

Thermodynamic Properties of Brayton Cycle

| Section | Temperature (°C) | Pressure (MPa) |
|---|---|---|
| 1 | 494 | 7.00 |
| 2 | 122 | 2.41 |
| 3 | 25 | 2.41 |
| 4 | 66 | 3.09 |
| 5 | 25 | 3.09 |
| 6 | 151 | 7.00 |
| 7 | 300 | 7.00 |

### V.C. Loss-of-Coolant Accident

In order to determine the appropriate response for a large-scale coolant accident, a thermal analysis of the core was performed under the conditions that would exist during a severe LOCA. A design basis complete LOCA was postulated. The break was assumed to be sufficiently large so that any helium in the core immediately escaped into the containment building, resulting in a rapid pressure drop (to 0 psig) and complete loss of normal core cooling. It was assumed that the neutron source was immediately shut down and that all heat addition came from decay heat calculated using the ORIGEN-S code. Figure 16 displays the decay heat for two different fuel compositions. C1 represents previous work on the GCFTR-2 with 100% TRU fuel being burned for 1825 days (Ref. 3). C2 represents the current work with an increased burnup of 3000 days and a new mixed fuel composition of 70% TRU/30% $^{238}$U. The difference in the decay heat can be attributed to the increase in burn time which provides for more fission products and actinides.

Once the coolant is lost, the only significant process for removing heat from the core is thermal radiation transfer. Because sophisticated computer modeling would be needed to simulate this process for the entire core, a comparison was made between the GCFTR-3 and the annular core of a helium-cooled prismatic fueled reactor (PFR) in which a detailed calculation of the amount of heat rejected from the core as a function of time had been made.[47] Although the PFR design differed in heat capacity, the general analysis was formulated as a hot surface radiating heat in which the time-dependent temperature of the PFR following a LOCA was already known, thus providing a means to estimate the capability of the core to radiate heat.

In order to adjust the PFR values for the GCFTR-3, a scaling factor based on geometry and the Stefan-Boltzmann Law was derived. The parameter included a multiplication constant of 2.2, which was taken as the product of a ratio of surface areas of the GCFTR-3 and PFR with a temperature ratio raised to the fourth power to compensate for the dependence of radiation transfer on temperature. The modified rejection heat was then subtracted from the GCFTR-3 decay heat to provide a value for the overall heat stored in the reactor core as a function of time.

Starting with a clad temperature of 831 K and using a core mass and specific heat of $6 \times 10^5$ kg and 600 J/kg K, respectively, the following equations were solved:

$$Q(t)_{core} = Q(t)_{decay} - Q(t)_{reject} = mc\Delta T$$

and

$$Q(t)_{reject} = 2.2\left(\frac{T_{\text{GCFTR-2}}}{T_{\text{PFR}}}\right)^4 Q(t)_{reject\_\text{PFR}} \ .$$

Starting with the inner clad temp based on thermal analysis of the core, the first change in temperature was calculated from the first equation. The rejection heat of the GCFTR-3 was estimated from the second equation by scaling the rejection heat from the PFR by a geometric factor and a factor based on the Stefan-Boltzman Law. The scaling factor was updated iteratively after 1-min

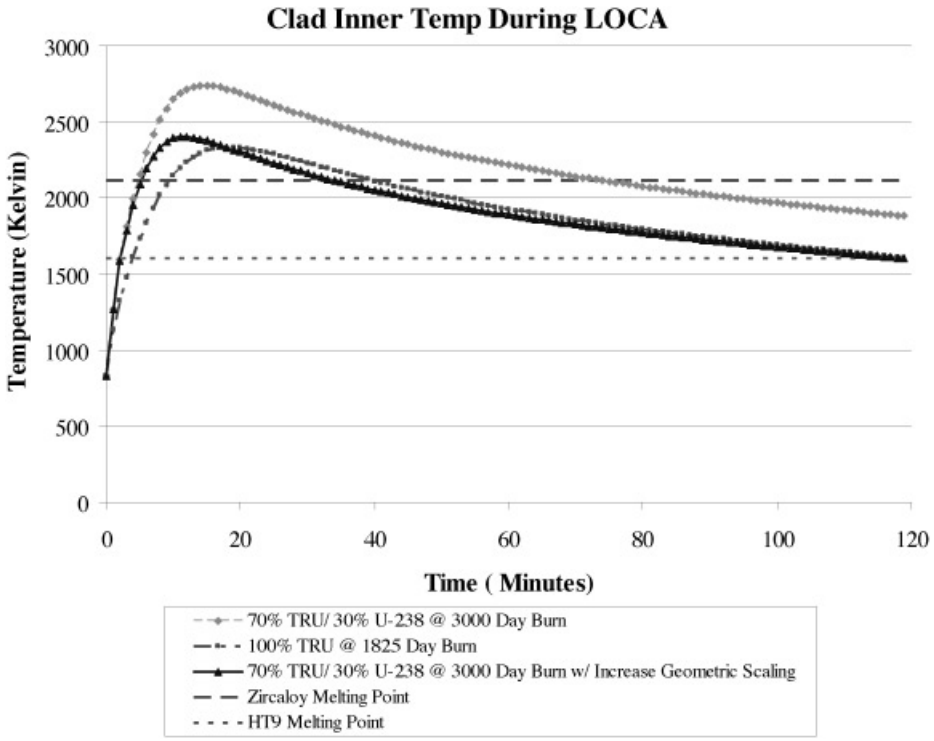


Fig. 17. Clad temperature during LOCA.

intervals at which time a new change in temperature was determined.

Figure 17 displays the temperature rise along with the melting temperature for two different clad materials. Without emergency core cooling it was determined that the core would experience significant damage two minutes after a complete loss of coolant. The clad temperature peaks soon after at 2465°C, at which point the core begins to radiate more heat than is accumulated from decay because of the dependency of radiative heat transfer on temperature.

In comparison with previous work[3] that calculated clad temperature during a LOCA by direct computer simulation, the current method for assessing a LOCA produces roughly similar time scales and temperatures. The overall melt times and maximum temperatures, however, cannot be accurately compared because of different burnup conditions used in the previous analysis. What can be concluded is that it becomes progressively harder to survive a LOCA as burn time is increased. For example, comparing the results for 1825- to 3000-day fuel burnups, the additional decay heat for the 3000-day burnup increases the clad temperature at every point by ~300°C relative to the values for the 1825-day burnup.

With the higher burnup it becomes extremely difficult to lower the core temperatures to a safe level. Even with the addition of large heat sinks which raise the average thermal capacity of the core, the time to melt still retains a value below 10 min. In order to reduce the maximum temperature or decrease the amount of time needed from an ECCS, the only parameter capable of significantly altering the temperature rise is the geometric scaling factor. By increasing the ratio of surface area from 2.2 to 4 as shown in Fig. 17, the maximum temperature decreases 330°C and the time needed from an ECCS is greatly reduced. These results suggest that an increase in the total surface area, either through the use of fins or an increase in volume, would help mitigate some of the damage inflicted by extreme temperatures and help reduce the load on an ECCS.

### V.D. Emergency Core Cooling System

Both the above LOCA analysis and a previous analysis[3] of the same core demonstrate that while long-term core cooling via only natural means (i.e., radiation and convection) is viable, the decay heat load immediately following a LOCA is high enough to initiate cladding failure in under 10 min. Consequently, a means of short-term emergency core cooling is necessary to ensure safe cladding temperatures under all conditions.

Consistent with passive safety design goals, an accumulator system was designed to provide emergency core cooling. The accumulator was engineered to meet several critical design criteria: passive actuation and injection, adequate coolant injection rates under all

credible core conditions (i.e., decay heat loads), and sufficient injection time to allow decay heat loads to reduce to safe levels.

The final accumulator design was a ring header in the shape of a torus, which can be located either above or below the reactor. Attached to the torus are twenty-four 55-$m^3$ standby helium tanks. The torus is connected to the reactor via four 15.24-cm (6-in.) inner diameter injection headers, each containing a flow restrictor and check valve in series, and the entire system is pressurized to 6.5 MPa. The accumulator system uses no components that require operator action or power and thus is considered a passive safety system. It uses no pumps, compressors, control circuitry, or power-operated valves. Under normal conditions, reactor pressure seats the check valves in the injection headers, thereby isolating the accumulator from the reactor.

Upon initiation of a LOCA, reactor pressure decreases rapidly. This drop in reactor pressure causes a difference between accumulator pressure and reactor pressure, thereby driving the helium in the accumulator into the reactor vessel via the natural pressure differential. Early in the accident sequence (when decay heat is high) the differential pressure between the accumulator and the reactor is also high, resulting in a high flow rate and heat removal rate (see Table XI). As the accumulator's helium supply is diminished, the driving pressure is also reduced and the injection rate will drop accordingly. The use of flow restrictors in the injection lines is critical to ensure that the helium supply does not deplete too quickly and that injection rates are appropriate for their corresponding decay heat loads.

The size of the accumulator, minimum coolant mass, flow restrictor properties, and standby pressure are primarily functions of the worst-case decay heat load and core flow parameters. First, a limiting clad temperature was selected; this value was determined to be 1500 K, ~100 K below the ODS clad melt temperature. Next, a convection coefficient, $h$, which would provide sufficient cooling to maintain this cladding temperature under the decay heat load at any given time, was calculated. Based on this convection coefficient, a Nusselt number and a Reynolds number for coolant injection were determined.[48] From the Reynolds number, a coolant velocity and mass flow rate were determined. The mass flow rate was used to determine a minimum adequate driving pressure and flow restrictor coefficient.[48] Each of these values was calculated at various points in time during the first 2 h of the LOCA. The mass flow rates were integrated to determine the necessary standby coolant mass, and the accumulator volume was selected to meet driving pressure requirements.

Various safety factors were applied to ensure appropriate margin (with respect to maximum cladding temperature) and to account for any design uncertainties. The decay heat loads were conservatively selected by modeling a burnup of 3000 days for the entire core, rather than just one fuel batch. This led to a substantial rise in decay heat over previous analyses[3] and provided a conservative bounding heat load for ECCS. Calculated convection coefficients were divided by a factor of 2 to account for any unforeseen reductions in coolant flow during the accident and to account for peaking factors. Finally, although LOCA analyses have shown that peak cladding temperatures approach (but do not exceed) the melting point, this condition exists for only a brief period of time. See Fig. 17.

Figure 18 demonstrates the effectiveness of the accumulator. Note that margin is maintained between peak cladding temperature (1500 K) and clad melt temperature (1600 K). Also of interest is that the accumulator system substantially suppresses cladding temperatures throughout the duration of the transient, thereby maintaining temperatures at safe values well beyond the point where peak cladding temperature is reached.

The ECCS coolant velocities and flow rates are given in Table XI, the calculated clad temperature versus time is shown in Fig. 18, and the temperature margin versus time is given in Table XII.

TABLE XI

ECCS Injection Velocities and Coolant Flow Rates

| Time After LOCA (min) | Coolant Velocity (m/s) | Coolant Flow Rate ($m^3$/s) |
|---|---|---|
| 1 | 17.33 | 66.00 |
| 5 | 16.81 | 63.95 |
| 10 | 16.30 | 62.10 |
| 15 | 16.03 | 61.08 |
| 30 | 14.49 | 55.13 |
| 45 | 12.93 | 49.19 |
| 60 | 11.63 | 44.27 |
| 90 | 8.14 | 30.95 |
| 120 | 0.25 | 27.46 |

## VI. FUSION NEUTRON SOURCE

### VI.A. Neutron Source Strength Capability

A neutron source design task for GCFTR-3 was to determine the maximum neutron source strength possible without changing the dimensions of the GCFTR-2 neutron source in order to allow operation at the lower values of $k_{eff}$ associated with higher fuel burnup. To this end, increases of normalized beta, $H$-factor, and current that can provide for an increase of fusion power up to ~500 MW were investigated. An in-house fusion performance code, based on the numerous engineering and physics constraints given in Ref. 49, was used for

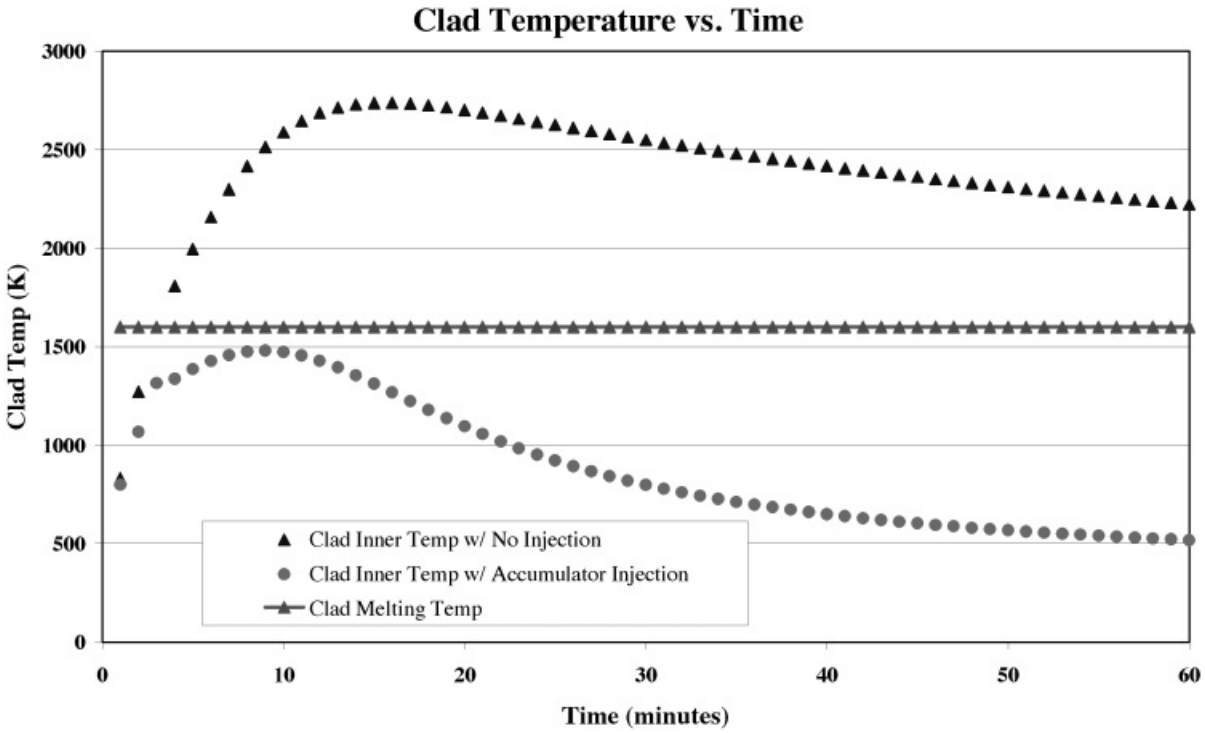


Fig. 18. ECCS effect on cladding temperatures.

TABLE XII

Clad Temperature Safety Margins

| Time after LOCA (min) | Cladding Temperature (K) | Margin ($T_{clad} - T_{melt}$) (K) |
|---|---|---|
| 5 | 1386.8 | 214.2 |
| 9 | 1479.9 | 120.1 |
| 15 | 1312.4 | 287.6 |
| 25 | 921.5 | 678.5 |
| 35 | 711.7 | 888.3 |
| 60 | 518.0 | 1082.0 |

systems analysis of plasma performance. Certain plasma and systems parameters were fixed, as indicated in Table XIII.

The target operating fusion power was 500 MW, which is large enough to sustain the 3000 MW(thermal) power in the fission reactor down to $k_{eff} \approx 0.5$ (see Sec. IV). The design of the tokamak fusion neutron source for the previous GCFTR-2 design[3] was based on normalized $\beta_N \leq 2.5$, $H$-mode confinement enhancement factor $H^{\text{ITER98}} \approx 1.0$ and plasma current $I = 8.2$ MA. The effects of modest increases of these parameters on fusion power were evaluated, subject to physics and engineering constraints.[49]

Figures 19 and 20 show how $\beta_N$ and the $H$-factor affect the total power and the required auxiliary power at currents of 9 and 10 MA, respectively, using the fixed parameters listed in Table XIII and the engineering and physics constraints in Ref. 49. Figure 19 shows that with a current of 9 MA, the maximum fusion power is ~400 MW, keeping within acceptable normalized beta and $H$-factor limits. Figure 20 shows that by increasing the current to 10 MA, a fusion neutron source power of 500 MW becomes possible. Table XIV shows

TABLE XIII

Constrained Parameters for Performance Evaluation

| Constrained Parameter | Value |
|---|---|
| Toroidal (major) radius (m) | 3.75 |
| Plasma (minor) radius (m) | 1.08 |
| Magnetic field of TF coil (T) | 11.8 |
| Plasma elongation | 1.7 |
| Plasma triangularity | 0.4 |
| % Greenwald density limit | 75 |
| Allowable field swing in CS (T) | 26.3 |

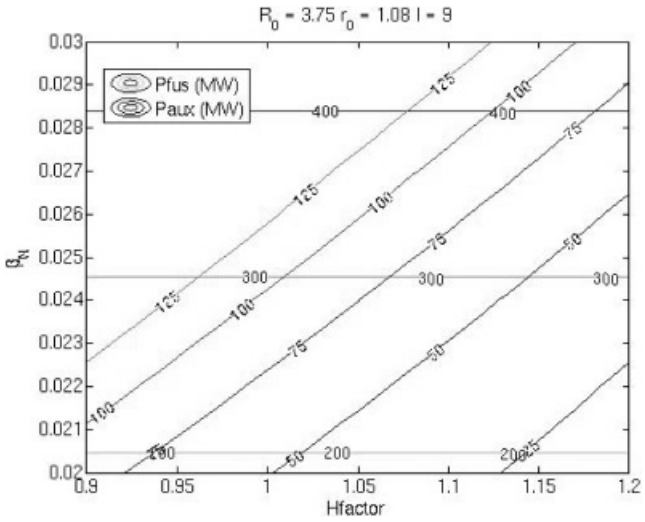


Fig. 19. Fusion power at $I = 9$ MA.

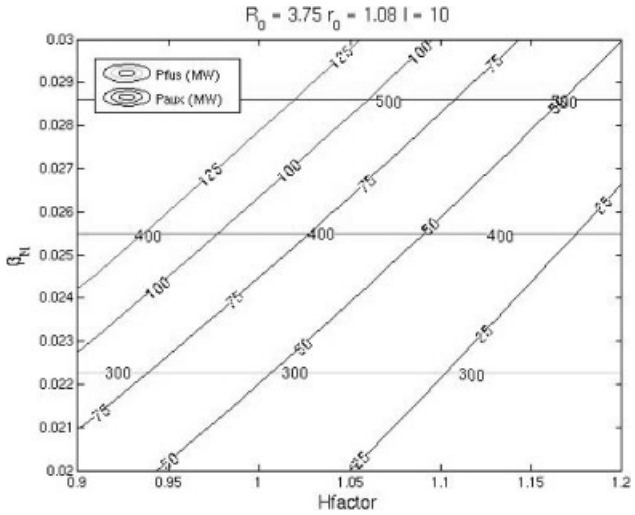


Fig. 20. Fusion power at $I = 10$ MA.

the plasma performance parameters calculated for these two cases using a normalized beta of 2.85%. Operating at lower currents requires increasing the *H*-factor in order to avoid the auxiliary power (design) limit of 100 MW. Table XIV shows that in order to meet this constraint the *H*-factor must be increased to 1.13 to operate at maximum power, which is an aggressive value and may not be possible. As a result, a current of 10 MA is probably necessary to meet the design objective of 500 MW of fusion power without exceeding 100 MW of auxiliary power.

### VI.B. Adaptation of ITER Divertor to Helium Coolant

#### *VI.B.1. Overview of Divertor*

The heat exiting the plasma across the last confined flux surface is swept along field lines into the divertor chamber and deposited over a relatively small area on the divertor target. This produces a very high heat flux on the divertor, of order 5 MW/m$^2$ for ITER and 1 to 2 MW/m$^2$ for GCFTR-3, during normal operation, with much higher peaks during disruptions. To handle this heat flux, the

TABLE XIV

Performance Characteristics for 9- and 10-MA Fusion Neutron Sources

| Plasma Parameter | $I_p = 9$ MA | $I_p = 10$ MA | ITER $I_p = 15$ MA |
|---|---|---|---|
| Total fusion power (MW) | 403 | 498 | 410 |
| Neutron source ($10^{19}$/s) | 14.2 | 17.5 | 14.4 |
| Auxiliary power (MW) | 98.6 | 98.2 | |
| Plasma power amplification, $Q_p$ | 4.1 | 5.1 | 10.0 |
| Normalized beta, $\beta_N$ (%) | 2.85 | 2.85 | 1.8 |
| Toroidal beta (%) | 4.036 | 4.485 | |
| *H*-factor | 1.13 | 1.06 | 1.00 |
| Energy confinement time (s) | 0.726 | 0.737 | |
| *L*-to-*H* threshold power (MW) | 27.1 | 28.73 | |
| Safety factor, $q_{95}$ | 5.472 | 4.01 | |
| Volt-seconds for startup | 98.5 | 107.3 | |
| Bootstrap current (MA) | 2.63 | 2.55 | |
| Current drive efficiency ($10^{-20}$A/W m$^2$) | 0.456 | 0.58 | |
| Electron density | $1.84 \times 10^{20}$ | $2.05 \times 10^{20}$ | |
| Toroidal magnetic field (T) | 5.9 | 5.9 | |
| Poloidal magnetic field (T) | 1.2 | 1.3 | |
| Neutron wall flux (MW/m$^2$) | 1.45 | 1.78 | 0.5 |
| FW heat flux (MW/m$^2$) | 0.32 | 0.35 | 0.15 |

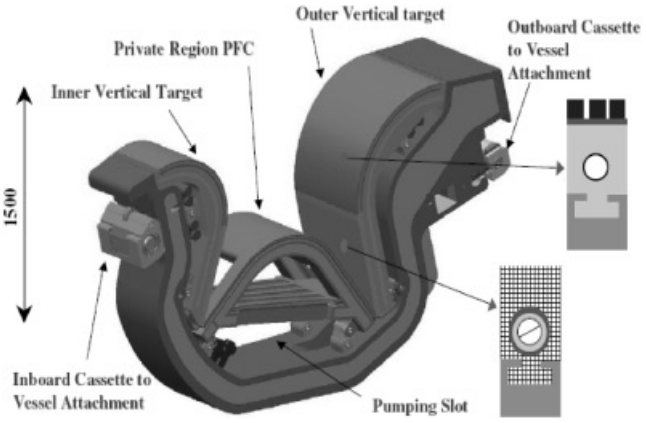


Fig. 21. Divertor cassette.[50]

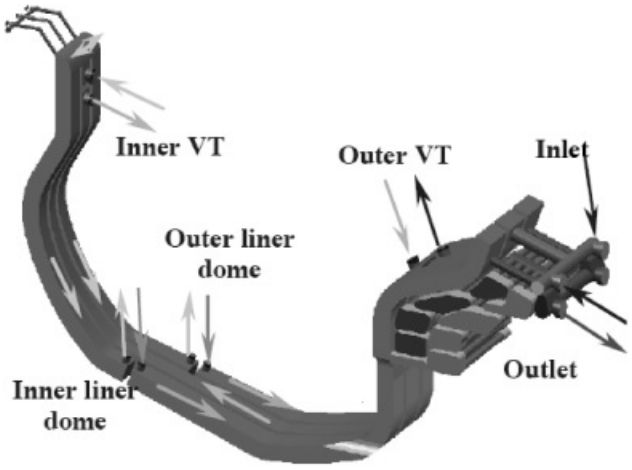


Fig. 22. Divertor coolant flow.[50]

ITER divertor[50,51] employs either carbon fiber, carbon, or tungsten tiles, joined to copper blocks. The copper blocks are hollow with a smooth tube or a swirl tape along the tube, allowing coolant to flow, and are assembled on the inner and outer vertical targets, as well as the divertor dome. For each of the 54 divertor cassettes, coolant flows in series first through the outer vertical target, then the inner vertical target, and then through the dome. Figure 21 shows a picture of a divertor cassette with a cross section of the copper block assemblies, and Fig. 22 shows the coolant flow through each cassette.

Water is the coolant for ITER, but because helium is the primary coolant for GCFTR-3, a thermal analysis to determine whether helium can cool the divertor was made. Adapting the coolant from water to helium has the main advantage of simplifying the plumbing for GCFTR-3 and avoids having different coolants for the fission and fusion components. In order to facilitate the adaptation to helium, the coolant flow for the GCFTR-3 will not be in series, as is the case for ITER, but will have individual coolant loops for the inner vertical target, outer vertical target, and dome.

### *VI.B.2. Thermal Analysis for Helium Coolant*

Divertor heat removal was modeled analytically, based on straight pipe flow that is a certain distance below a uniform heat flux. Heat removal was also analyzed in three dimensions using Fluent,[52] which solves the energy equation coupled with the Navier-Stokes equations. A 3-D model and mesh for one cooling channel of the outer vertical target, created using Gambit,[52] consists of a copper block with a smooth tube. The analytical calculations of the maximum surface temperature of the block and average coolant exit temperature, when cooling with water, agreed with those of ITER (Ref. 51), giving confidence in using the model to analyze helium. However, operating conditions for helium differ somewhat from water, in that the operating pressure increases from about 4 to 6.5 MPa, helium inlet temperature is 300 K, and helium mass flow rates vary from 0.4 to 1.2 kg/s.

The maximum surface temperature of the copper block was a major design constraint in the analysis of the coolant channel. Figure 23 shows the Fluent results of peak surface temperature on the copper block for the mass flow and heat flux region analyzed. The heat flux was modeled as a uniform heat flux on the entire plasma-facing surface with the initial conditions mentioned previously. Each mass flow rate case was run for seven different heat flux values ranging from 0.5 to 2 MW/m$^2$. 773 K was the maximum allowable surface temperature based on literature studies[53]; 696 K and 579 K represent

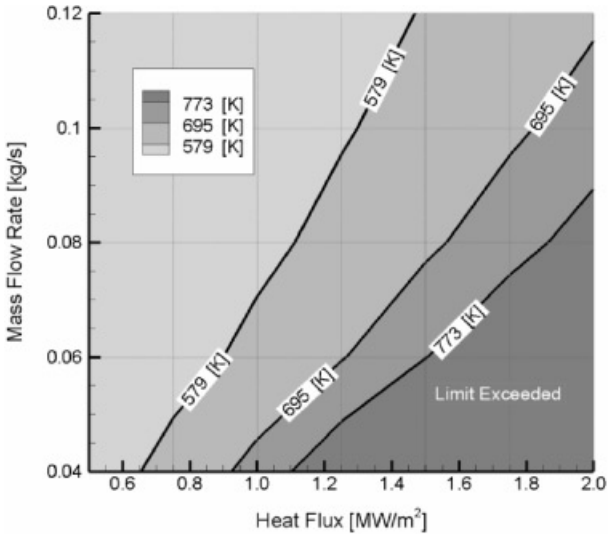


Fig. 23. Maximum surface temperature.

90% and 75% of the limit, respectively. The Fluent results agreed well with parallel analytical calculations. As Fig. 23 shows, using a uniform heat flux approximation results in an achievable heat removal for the 0.5 to 2 MW/m$^2$ divertor heat flux range anticipated for normal operation of GCFTR-3.

The mass flow rate range analyzed corresponds to an inlet velocity range of 60 to 190 m/s. This velocity could be reduced by increasing the cross-sectional area of the channel. For this study, the flow tube is 10 mm in diameter, maintaining ITER's dimensions. The Fluent results show that a channel could sustain 1 MW/m$^2$ and avoid failure at the 60 m/s inlet velocity range, while an inlet velocity of 143 m/s would be required for 2 MW/m$^2$.

Based on the pressure drop across the channel that Fluent converged upon, the pumping power per channel was calculated. This calculation indicates that a 1 MW/m$^2$ heat flux at 0.04 kg/s would require approximately 250 W, and a 2 MW/m$^2$ heat flux at 0.1 kg/s would require 4.8 kW, per channel. The ratio of the pumping power to the total heat removed per channel (assuming an 85% pumping efficiency) results in 0.5% and 6.1% for the 1 and 2 MW/m$^2$ cases, respectively. To estimate the pumping power for GCFTR-3, these values were scaled up based on the total number of channels. This yields a total pumping power of approximately 511 kW and mass flow rate of 89 kg/s for the 1 MW/m$^2$ heat flux and 10.6 MW with 222 kg/s for the 2 MW/m$^2$ heat flux. This may be somewhat low since the center dome will require a larger pumping power than the outer targets.

Using results from both the analytical calculations and the Fluent model of the outer vertical target, approximate values were found for the effect of heat transfer enhancement by swirl tape. The enhancement multiplication factors used were 2 for the friction factor and 4 for the convective heat transfer coefficient.[54] These factors only represent a rough approximation of the effect, because of the limited capability of the analytical solution and their uniform application. The solution procedure involved iteration on the friction factor using the Colebrook formula and the Petukhov correlation for Nusselt number.[54,55] This created a reduction in the required mass flow rate by ~45%, and thus a reduction in the pumping power needed to handle the required heat flux loads.

The center dome region of the divertor is ~0.8 m longer than the outer vertical target and thus presents a more limiting case. The analytical model indicates that an ~25% increase in mass flow rate would be required to sustain the same heat flux relative to the outer vertical target. The use of swirl tape or other heat transfer enhancement methods would improve the operating limits for the center dome.

Based on this analysis, it seems feasible to adapt the ITER divertor design for use in GCFTR-3 using helium as the coolant.

### VI.C. H&CD Systems

The proposed ITER H&CD systems[56,57] incorporate all major electromagnetic wave H&CD systems in use today. Selected components of ITER's systems were implemented in GCFTR-3 because of their desirable properties and GCFTR-3's design constraints. This section focuses on required properties of GCFTR-3's H&CD system and a description of how ITER's H&CD system was adapted for use in GCFTR-3.

#### *VI.C.1. Current Drive Requirements*

An important part of the GCFTR-3 current drive requirement is the bootstrap current. Since GCFTR-3 is to operate in steady state, it is mandatory that noninductively driven current plus bootstrap current be equal to the total required plasma current of 9 to 10 MA. The required noninductively driven current is $I_{cd} = (1 - f_{bs})I_p$. With all the auxiliary power available for current drive and allowing the current drive to be described by the current drive figure of merit[58] as follows:

$$\gamma_{cd} = \bar{n}_{e20} R_0 (1 - f_{bs}) I_p Q_p \frac{1}{P_{fus}} \ ,$$

we can determine a necessary parameter of our H&CD system.

An empirical formula for the bootstrap current fraction (of the plasma current) is given by the following expression[58]:

$$f_{bs} = \left( 1.32 - 0.235 \left( \frac{q_{95}}{q_0} \right) + 0.0185 \left( \frac{q_{95}}{q_0} \right)^2 \right) \times \left( \sqrt{\frac{1}{A}} \beta_p \right)^{1.3} \ .$$

In these formulas,

$n_{e20}$ = plasma electron density in units of $10^{20}$/m$^3$

$R_0$ = major radius from the vertical centerline of the reactor (see Fig. 1) to the toroidal centerline of the plasma chamber

$I_p$ = plasma current in MA

$Q_p$ = plasma heat energy multiplication factor due to fusion

$q_x$ = plasma safety factor evaluated at the major radius ($x = 0$) or the outer plasma radius ($x = 95$)

$A = R_0/a$, with a being the minor plasma radius from the toroidal centerline to the outside of the plasma

$\beta_p$ = ratio of the kinetic plasma pressure to the pressure in the poloidal magnetic field formed primarily by the plasma current.

These formulas are used to evaluate the current drive requirements for the 500-MW(thermal) GCFTR-3 tokamak.

The required bootstrap current fraction in GCFTR-3 at steady-state, 500-MW(thermal) operation is ~0.25. By comparison, a conservative ITER design value is ~0.5. The bootstrap current for the GCFTR-3 is reasonably achievable by today's standards. Bootstrap currents as high as 80% have been achieved at low performance in JET (Ref. 58) and JT-60U (Ref. 59).

### *VI.C.2. GCFTR-3 500-MW(thermal) H&CD Requirements*

The current goals of the GCFTR-3 design include power levels that require nontrivial H&CD injected power. It was determined that 100 MW of concurrent power delivery was a reasonable design limit, given technology levels, electrical power availability, and plasma access limits. With the goal of increasing the tokamak fusion power to 500 MW(thermal), an H&CD system was researched in order to increase H&CD capabilities while meeting the operational requirements and design constraints of the higher-output tokamak.

An important type of H&CD system is neutral beam injection (NBI). However, because of the size, geometric requirements, and complexity of this type of system, it was excluded from consideration. Current drive, which is critical to the operation of GCFTR-3, requires the NBI system to be aligned tangential to the plasma axis. This proves very difficult and impractical with an annular fission reactor surrounding the plasma chamber. Therefore, it was decided to focus on systems that simultaneously provide H&CD while geometrically perpendicular to the plasma axis.

The H&CD requirements are determined to support a fusion neutron source operating at the upper limit believed feasible for the present design (Sec. VI.A). Several aggressive parameter values were used in the pursuit of this goal in the design. A main parameter increased over past designs is the plasma current. This performance increase raises the requirements of the H&CD system. It is this increase that demands the high current drive figure-of-merit lower hybrid (LH) system over other more well-known systems. Also, the heating power input was augmented to a continuous maximum of 100 MW with a peak output of 120 MW, another aggressive value demanding six 20-MW LH H&CD units. A third demand was to fit H&CD systems between TFCs and include shielding. An LH H&CD system provided the correct size, power, and the highest achieved current drive efficiency, albeit being inferior in achieved heating.

The required current drive figure of merit for the LH H&CD system at 500 MW(thermal) fusion power, 10 MA of current, and a bootstrap current fraction of 25% is 0.577. In 2000, current drive figures of merit as high as 0.45 were achieved with an LH and ICRF dual-resonance H&CD system.[56] Therefore, with near-term technological advances, expecting the H&CD system to be capable of fulfilling GCFTR-3 design requirements is reasonable. Additionally, higher bootstrap current will be achieved in the future, easing the wave current drive requirements.

The actual LH port designs are based on the port plugs used in the ITER ion cyclotron resonance heating (ICRH) system. Each port has a power of 20 MW. In GCFTR-3, there are two sections of the annular fission reactor between the magnets removed on opposite sides of the reactor. This design is based on the need for H&CD system access to the plasma. Because of the highly constrained geometric options, the six 20-MW LH port plugs are centered vertically and toroidally in the outer plasma chamber wall in an arrangement like the one in Fig. 24, with three in each removed reactor section. This type of arrangement has not been extensively tested in tokamaks, but is mandatory in order to provide the required amount of H&CD and allow for magnet shielding in GCFTR-3. Based on the ITER designs, it is expected that each LH H&CD port would provide 20 MW of heating and ~1.5 MA of current drive.[57] Table XV shows a comparison for the GCFTR-3 and ITER H&CD systems. Note that the GCFTR design used an LH system with a power flux of 33 MW/m$^2$, while the ITER ICRH system has a power flux of 9 MW/m$^2$.

Since LH H&CD systems are currently the least efficient for heating, it is important to consider a secondary system. As LH systems are the most effective at driving current, an integral component for GCFTR-3 operation, the secondary system will not satisfy the required specifications with current or near-term technology. However, until research either improves LH heating efficiency or improves the current drive performance of the other two main systems, a secondary H&CD capability must be considered.

The most promising H&CD system in terms of plasma heating is the ICRH system. However, as ICRH H&CD systems only provide $0.15 \times 10^{-20}$ A/W m$^{-2}$ of current drive compared to 2 to $3 \times 10^{-20}$ m$^{-3}\cdot$A/W in LH systems,[58] more development is needed before the ICRH wave can fulfill GCFTR-3's requirements for steady-state operation. Another challenge in implementing ICRH H&CD systems is their large size. The ICRH launchers deliver a power density of 9.2 MW/m$^2$ compared to 33 MW/m$^2$ for LH launchers. The larger ICRH launchers would still be able to fit between the magnets at the plasma chamber-reactor interface, but the shielding for the magnets would have to be significantly reduced. A

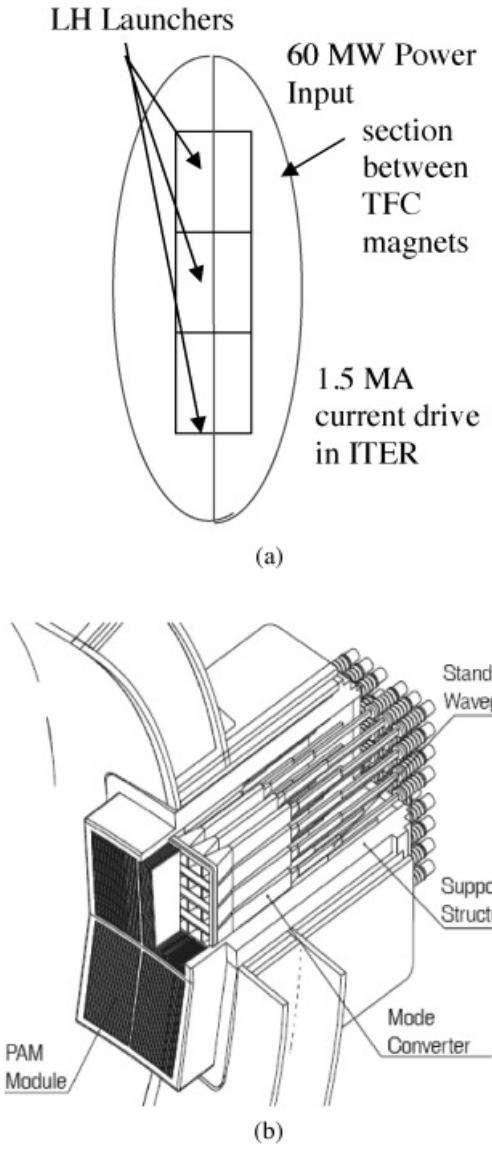


Fig. 24. (a) LH port geometry[56]; (b) LH Launcher.[56]

launcher redesign would have to be completed to accommodate ICRH heating and reduced shielding. However, a backup ICRH system could be realized with reasonable improvements in performance.

### VI.D. Superconducting Magnet System

The GCFTR-3 magnet system is directly based upon the ITER design.[60,61] The magnet system consists of three main sets of magnets: the CS, the TFCs, and the poloidal field coils (PFCs). Each of these systems can be seen in Fig. 1. Only the first two systems will be discussed. The previous GCFTR-2 design[3] has set some preliminary values for the magnet systems. These values must be revised, as the GCFTR-3 will use an increased plasma current of 10 MA.

TABLE XV

GCFTR-3 H&CD Properties

| Property | GCFTR-3 (LHR) | ITER (ICRH) |
|---|---|---|
| Bootstrap current | 2.5 MA | ~7.5 MA |
| Fractional bootstrap current | 25% | ~50% |
| Plasma current | 10 MA | 15 MA |
| Maximum simultaneous H&CD power | 100 MW | 110 MW |
| Total H&CD capacity | 120 MW | 130 MW |
| Number of port plugs | 6 | 10[a] |
| Power density | 33 MW/m$^2$ | 9.2 MW/m$^2$[b] |

[a]4 equatorial, 3 upper, 3 NBI.
[b]ICRH power density in generic 20-MW port.

The CS for the GCFTR-3 is directly adapted from ITER and uses a cable-in-conduit $Nb_3Sn$ conductor surrounded by an Incoloy 908 jacket. The superconductor is cooled through a channel carrying supercooled helium in the center of the cable-in-conduit. The CS creates a magnetic flux that inductively starts the plasma current and ohmically heats the plasma. It operates with a maximum magnetic field of 13.5 T. The two main dimensions of the CS are the flux core radius and the thickness. These two factors are constrained by the amount of inductive start up volt-seconds needed, and by the maximum allowable stress in the CS, respectively. A goal of this project was to leave the size of the GCFTR-3 the same as the previous design, the GCFTR-2. The GCFTR-2's dimensions were analyzed to see if they could meet the new requirements of the GCFTR-3. This constrained the total flux core radius plus thickness of the CS not to exceed 1.36 m. The increase in plasma current to 10 MA forced the requirement for the inductive start volt-seconds, $VS_{start}$, to increase from the previous design value based on 8.3 MA of plasma current. The required $VS_{start}$ was a minimum of 107.3 volt-seconds, found using Ref. 49. $VS_{start}$ was constrained using the following equation[49]:

$$\pi \cdot \Delta B_{OH} \cdot R_v^2 \left[ 1 + \frac{\Delta_{OH}}{R_v} + \frac{1}{3} \cdot \left( \frac{\Delta_{OH}}{R_v} \right)^2 \right] \geq VS_{req\text{-}start} \ ,$$

where

$$\Delta B_{OH} \cong 2 \cdot B_{OH}^{max} = 27 \text{ T}$$

$R_v$ = flux core radius in meters

$\Delta_{OH}$ = thickness of the CS.

A configuration of a flux core radius of 0.88 m and a CS thickness of $\Delta_{OH} = 0.48$ m created a $VS_{start}$ of 108 V-s, satisfying the minimum needed, as well as leaving the total radius at 1.36 m. The stress in the CS was approximated using the following equation[49]:

$$\sigma = C \cdot \frac{1}{f_{structure}} \cdot \left( \frac{B_{OH}^2}{2 \cdot \mu} \right) \cdot \left( \frac{R_v}{\Delta_{OH}} + \frac{1}{3} \right) ,$$

where

$C$ = scaling constant equal to 1.4

$\mu$ = permeability constant

$B_{OH}$ = 13.5 T = maximum magnetic field in the CS

$f_{structure}$ = volume fraction of the conductor.

The $f_{structure}$ constant was calculated by determining the volume fraction of structural material in the conductors to the volume of the entire conductor as set by the original GCFTR design. The conducting strands have an internal diameter of 38 mm of conducting material and coolant chamber, surrounded by a 51-mm square of structural Incoloy 908. The value of $f_{structure}$ is 0.564. The maximum stress allowable in the CS, by ITER standards and Incoloy 908 limitations, is 430 MPa (Ref. 60). When using a flux core radius of 0.88 m and thickness of 0.48 m, the stress created is ~399.9 MPa. This is very close to the limit; therefore any increase in plasma current above 10 MA would require a thicker CS to reduce the stress.

The TFCs are designed using ITER (Ref. 60) as a basis. The GCFTR-3 uses a $Nb_3Sn$ cable-in-conduit superconductor with an Incoloy 908 jacket for support, as ITER does. These are also cooled through a channel carrying supercooled helium in the center of the cable-in-conduit. The GCFTR-3 will only use 16 TFCs to create the toroidal magnetic field for the plasma. The thickness of the TFC for GCFTR is determined by conserving the tensile stress calculated in the same manner for the ITER TFC. The tensile stress is approximately equal to the magnetic force/cross-section area, or $s = F/A = (C \cdot I_{TF}^2/A)$. Keeping the stress constant, the area of the GCFTR-3 TFCs is found when the ITER parameters[60] of a coil current of 9.13 MA and area of 0.3 $m^2$ are used. The TF coil current needed in the GCFTR-3 is calculated using Ampere's Law:

$$I_{TF} = \frac{B \cdot 2 \cdot R}{\mu_0 \cdot N} ,$$

where

$B$ = magnetic field at the conductor

$R$ = radius at the conductor

$N$ = number of TFCs.

The magnetic field on the major axis of the plasma is related to the magnetic field at the TF conductor[49] by

$$B = B_{TFC} \left( \frac{R_v + \Delta m}{R_O} \right) ,$$

where

$B_{TFC}$ = maximum magnetic field in the TFCs

$R_O$ = major radius

$\Delta m$ = radial thickness of the CS and TFC.

This magnetic field is calculated so that the current inside the conductor can be calculated. From this current we are able to calculate the required area by keeping the stress constant from ITER. Using these equations the area of the TFCs for the GCFTR-3 comes out to 0.1567 $m^2$. Keeping the radial thickness of the TFCs the same as the previous design of 0.43 m requires the TFCs to have a new width of 0.3645 m in the toroidal direction. The new width of the TFCs was checked and approved using a CAD model to make sure that 16 TFCs would fit around the CS without overlap.

In conclusion, the magnet system of the GCFTR-3 is based on a scaling down of ITER and the GCFTR-2 designs. The increase in plasma current from 8.3 to 10 MA required an increase in flux core radius to 0.88 m to acquire an adequate start-up volt-seconds. The thickness of the CS coil was reduced to 0.48 m to conserve the size of the GCFTR-2 design. This thickness creates stresses in the CS very close to that of the maximum allowed in the ITER design, but is within the limit. The area of the TFCs needs to be greater than originally allowed in the GCFTR-2 design due to the increase in plasma current. In order to keep the radial thickness of the TFCs constant at 0.43 m, the width was increased to 0.3645 m. This new width still allowed 16 TFCs to surround the CS.

## VII. FUEL CYCLE

### VII.A. Objective

The goal of the GCFTR is to achieve a "deep-burn" (>90%) TRU burnup, if possible without the reprocessing of the fuel in the TRISO-coated fuel particles. The TRU comes from LWR spent fuel.[3] The goal is to reduce the actinide inventory so as to decrease the need for high-level-waste repositories of SNF such as Yucca Mountain. Previous studies[3,4,7] indicate that this deep burn is feasible via the use of repeated cycling of the TRU with reprocessing and adding more fissile TRU to keep the $k_{eff}$ of the system above ~0.8. Without reprocessing, the negative reactivity penalty introduced by the buildup of fission products and transmutation of fissile material would limit the practical burnup to ~15% with a 200-MW limit on the fusion power, and hence on the strength of the

fusion neutron source.[7] Two approaches to extend the burnup of the TRU from SNF in GCFTR-3 without reprocessing are reported in this paper: (a) lengthening the achievable fuel cycle by increasing the fusion neutron source strength to compensate a larger reactivity decrement (Sec. VI), and (b) admixing $^{238}U$ with the TRU in order to continuously produce TRU to reduce the reactivity decrement. With the addition of $^{238}U$ in the fuel to produce TRU, the quantification of the deep-burn goal becomes less clear-cut, and the concept of "uranium utilization" (how much of the energy content of the original uranium is utilized to produce electricity) may be a better characterization of the objective.

### VII.B. Fuel Batching

In keeping with previous GCFTR fuel cycle analyses,[3,4,7] the reactor core has been divided into five equal-volume annular regions. For the purposes of this analysis, each region is assumed to contain a uniform but time-dependent material composition throughout. Several shuffling patterns have been previously analyzed,[7] though this report will focus on the "out-to-in" pattern. The first five reactor cycles for a new reactor starting up and utilizing this concept are shown in Fig. 25. Initially, fresh fuel is placed into all five core regions and this configuration is burned for one cycle. At the conclusion of the first cycle, the fuel assemblies in the region closest to the fusion source are removed, all other assemblies are shifted one region inward, and a batch of assemblies with fresh TRU fuel is introduced into the outermost region. This process is repeated for three subsequent cycles until a configuration is obtained (last row in Fig. 25) in which at BOC the outermost region contains fresh fuel, the adjacent region contains once-burned fuel, the next region contains twice-burned fuel, the next region contains thrice-burned fuel and the innermost region contains fuel that is burned four times. Subsequent cycles would be identical to the cycle indicated by the fifth row in the figure, which is referred to as the steady-state cycle. This "five-batch, once-through" fuel cycle is the basis of the analysis in this section.

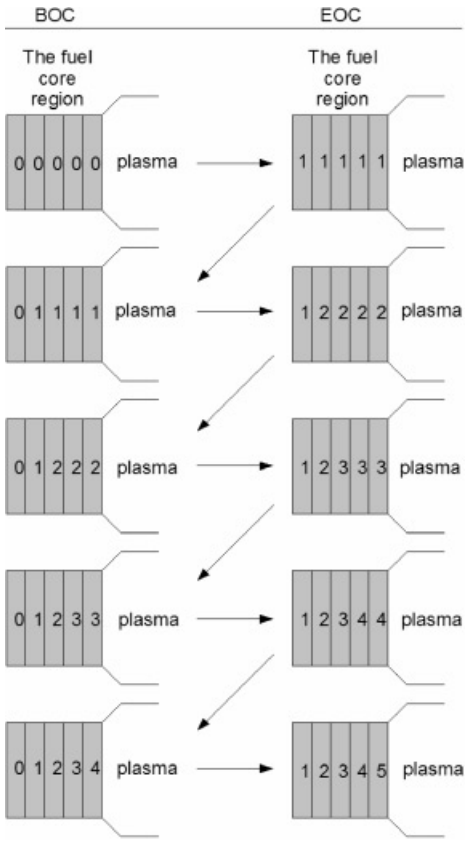


Fig. 25. Approach to steady-state fuel cycle.

Previous studies[3,4,7] have primarily focused on fuel cycles involving recycling and reprocessing of TRU fuel in order to achieve burnup goals. In contrast, this work focuses on the potential of a once-through cycle to achieve a significant burnup of actinides. The term "once-through" designates a fuel cycle in which an assembly will be irradiated once in each of the five regions of the reactor, at which point in time it will be permanently removed from the reactor. The total irradiation time experienced by an assembly is therefore five times the length of a single operating cycle, and this total irradiation interval will be referred to as the residence time of an assembly. After removal, an assembly may be designated for disposal in a permanent repository or it may be recycled further in a different reactor, but it will not return to the GCFTR.

### VII.C. Methodology

In order to conduct the analysis, the TRITON (Ref. 62) and EVENT (Ref. 38) codes were implemented. EVENT is a deterministic neutron transport code which is used in the determination of the multiplication factor of the system and in producing the neutron flux distributions. TRITON is a code which couples a deterministic transport solver with the depletion code ORIGEN-S (Ref. 6). It was used to simulate the irradiation of the actinide fuel to determine variations in the material composition over time. The CSA sequences[63] were used in order to create cross-section libraries for use by EVENT. Although the SCALE package is primarily used in the analysis of thermal reactors, the use of the 238-group library provides the capability to treat fast spectrum assemblies as well. All analyses performed on collapsed spectra were collapsed from this 238-group library based on realistic energy distributions calculated for the GCFTR.

To conduct an initial depletion for the purpose of establishing compositions for the cross-section generation, the power distribution across each of the five annular regions was assumed to be flat (i.e., each produced

20% of the power). The TRITON code was implemented, depleting the TRU fuel based on a simplified pin cell geometry which recalculates the energy distribution of the flux approximately four times per operating cycle as it depletes the fuel. This calculation was performed for the entire residence life (five operating cycles) of a fuel assembly. The 238-group cross-section set in the SCALE library (14 MeV to thermal) was used to calculate 238-group spectra (Fig. 12) that were automatically collapsed to the three groups that ORIGEN uses for the burnup calculation and to 27-group cross sections used in EVENT for the power distribution calculation.

In the EVENT model the materials were placed in the core in the reference out-to-in shuffle pattern, where for this case the composition of fresh fuel was placed in the outermost region, the composition after one cycle was placed in the second region, after two cycles in the third region, etc. At this point the compositions are only a rough estimate because of the starting assumption of a flat power distribution. A fixed-source EVENT run, with the fusion neutron source modeled as a volumetric source located throughout the plasma, was performed, and the resulting flux profile was obtained for both BOC and EOC conditions. It was then assumed that the power distribution in the core would be proportional to the flux distribution. While the power distribution is actually proportional to the sum over groups of the product of the macroscopic fission cross section and the group flux in each region, this assumption is a reasonable approximation as long as the energy dependence of the fission cross sections is not highly spatially dependent. Proceeding with this approximation, the relative magnitudes of the fluxes for a new burnup history for the fuel was created. The original depletion calculation was repeated, but now instead of assuming a constant power over the residence time, the new power distribution obtained from EVENT is used. The average power that is experienced by an assembly over its residence remains the same, only it is now burned at a variable power throughout its life. The rest of the calculation was carried out in exactly the same manner with the new fuel compositions for the second pass through the procedure. This process was repeated until the compositions resulting from subsequent passes showed little variation.

### VII.D. Cycle Length

It has been shown[7] that a burnup of 90% FIMA cannot be achieved in a once-through cycle without a fusion neutron source that is larger than has been used in previous GCFTR designs (200 MW). Therefore, this analysis was intended to identify the maximum burnup that can be achieved within a single (five-batch) residence time in a steady-state (row 5) fuel cycle, while adhering to the restrictions given by the fusion neutron source as described in Sec. VI. The minimum multiplication factor that can be accepted is primarily dependent on the strength of the fusion source supplying neutrons to the system. As argued in Sec. IV, a fusion source of 200 MW will allow a thermal output of 3000 MW to be sustained at a $k_{eff}$ value as low as ~0.8. Increasing the fusion source to 500 MW, which was supported by the analysis in Sec. VI, would allow for operation at 3000 MW(thermal) fission power at a subcritical multiplication factor of ~0.5.

In a steady-state cycle (row 5 in Fig. 25), fuel is present in the reactor at BOC that has already been irradiated for one-, two-, three-, and four-burn cycles. Thus, lengthening the fuel cycle means that all previously burned fuel will have been burned longer and hence will be less reactive, resulting in a lower $k_{eff}$ of the reactor as a whole. In order to maximize burnup in this once-through five-batch cycle, it is necessary to determine the cycle length for which the EOC $k_{eff}$ is at the lower limit that can be sustained by the fusion neutron source. It should be noted that the cycle length which can be sustained in a once-through cycle for pure TRU fuel is longer than that for an equilibrium cycle without reprocessing[7] (i.e., a fuel cycle in which batches are recycled >5 times without reprocessing), because less reactive fuel that had been burned more than five times would be present in the equilibrium fuel cycle. As is illustrated in Fig. 26, as TRU is irradiated not only does the primary fissile material, $^{239}$Pu, deplete, but neutron poisons such as $^{240}$Pu accumulate. This means that any equilibrium fuel cycle will inevitably tend toward a less-reactive composition, resulting in a shorter operating cycle for a given limit on $k_{\min}$ (Ref. 7).

The same basic steady-state fuel cycle calculation described above for a 600-day cycle length was repeated for cycle lengths of 1200, 1800, and 2400 days. Table XVI provides a comparison of several pertinent parameters for each of the cycle lengths analyzed. As discussed earlier, increasing cycle time not only increases the decrement in the $k_{eff}$ over the course of a cycle, it also decreases the BOC $k_{eff}$ that can be achieved and thus places a larger

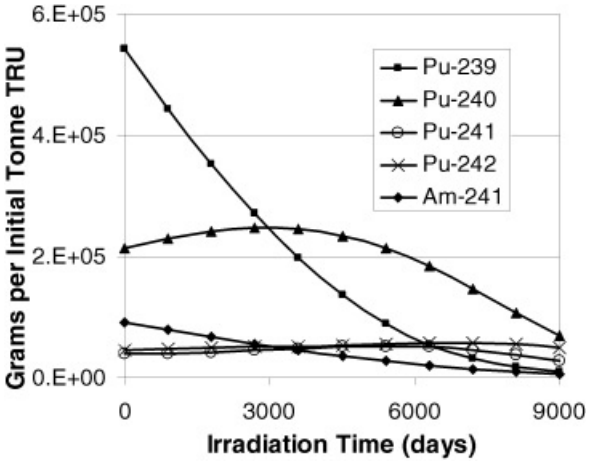


Fig. 26. TRU isotopic composition for $P \approx 86$ MW/metric ton HM.

TABLE XVI

GCFTR-3 Steady-State Fuel Cycle Parameters for Different Cycle Lengths

| Parameter | Cycle Length | | | |
|---|---|---|---|---|
| | 600 Days | 1200 Days | 1800 Days | 2400 Days |
| Thermal power (MW) | 3000 | 3000 | 3000 | 3000 |
| Cycles per residence time | 5 | 5 | 5 | 5 |
| Five-batch residence time (yr) | 8.2 | 16.4 | 24.7 | 32.9 |
| BOC $k_{eff}$ | 0.987 | 0.917 | 0.856 | 0.671 |
| EOC $k_{eff}$ | 0.927 | 0.815 | 0.714 | 0.611 |
| BOC $P_{fus}$ (MW) | 13 | 83 | 144 | 329 |
| EOC $P_{fus}$ (MW) | 73 | 185 | 286 | 389 |
| TRU BOC loading (MT) | 37 | 37 | 37 | 37 |
| TRU burned per year (metric tons/EFPY) | 1.12 | 1.12 | 1.09 | 1.05 |
| TRU burned per residence (MT) | 9.2 | 18.4 | 26.8 | 34.7 |
| TRU burned per residence (%) | 24.9 | 49.7 | 72.4 | 93.7 |
| SNF disposed per year (metric tons/EFPY) | 100.8 | 100.7 | 97.7 | 94.9 |
| Average core flux across cycle (n/cm$^2$-s) | 5.91E+14[a] | 7.09E+14 | 8.67E+14 | 1.01E+15 |
| Average fast (>0.1 MeV) flux (n/cm$^2$-s) | 2.66E+14 | 3.26E+14 | 3.90E+14 | 4.15E+14 |
| Fluence per residence time (n/cm$^2$) | 1.53E+23 | 3.68E+23 | 6.74E+23 | 1.05E+24 |
| Fast (>0.1 MeV) fluence per residence (n/cm$^2$) | 6.89E+22 | 1.69E+23 | 3.03E+23 | 4.31E+23 |

[a]Read as $5.91 \times 10^{14}$.

burden on the fusion source over the entire length of the cycle.

From this analysis, it appears that the availability of a fusion neutron source on the order of 500 MW would greatly enhance the burnup capability of a once-through transmutation cycle, though other issues begin to arise with these longer fuel cycles. As the operating *k*-effective is allowed to decrease, the location of the peak flux within the reactor core begins to shift significantly towards the fusion source (located to the left of region 1) as illustrated in Fig. 27. In the case of a 2400-day cycle, the flux is peaked dramatically towards the plasma region, producing a peak to average ratio of ~2.3, which is probably unacceptable. Examination of conventional methods (fuel zoning, burnable poisons, etc.) to reduce power peaking is beyond the scope of this study, but it can be anticipated that such measures could reduce the power peaking to an acceptable value.

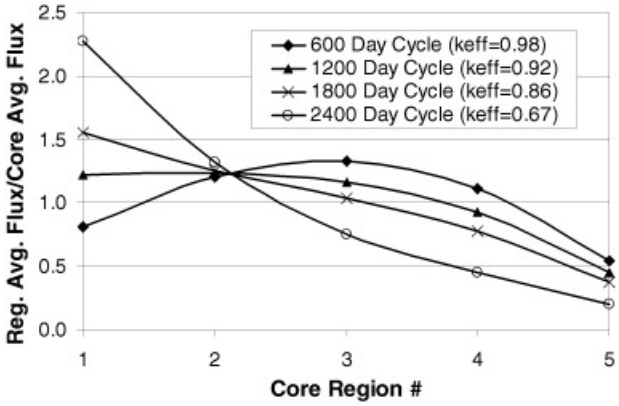


Fig. 27. BOC radial flux distribution.

Thus, it seems likely that the burnup goal of >90% burnup could be achieved in a once-through fuel cycle without reprocessing, provided of course that the TRISO fuel particles and cladding could survive the radiation damage associated with a fast neutron fluence of $>4 \times 10^{23}$ n/cm$^2$.

### VII.E. Fertile Admixing

In order to prevent the drop in the multiplication factor that results from a deep burnup of the fuel, the possibility of admixing fertile material in the form of $^{238}$U with the normal TRU fuel composition was considered. Although the presence of fertile material initially displaces fissile material, the potential slower decrement in $k_{eff}$ that would be experienced because of breeding of new fissile material might offset this adverse effect.

The primary analysis concerning the admixing of fertile material was performed for an infinite lattice of TRU fuel pins over a wide range of fertile concentrations. For the results shown in Fig. 28, each case contains the same overall mass of heavy metal (TRU + $^{238}$U), and the fertile additions listed represent weight percentages [$M_{238}/(M_{238} + M_{TRU})$]. Furthermore, the multiplication factor is calculated for an initial composition of entirely fresh fuel that is depleted uniformly throughout the

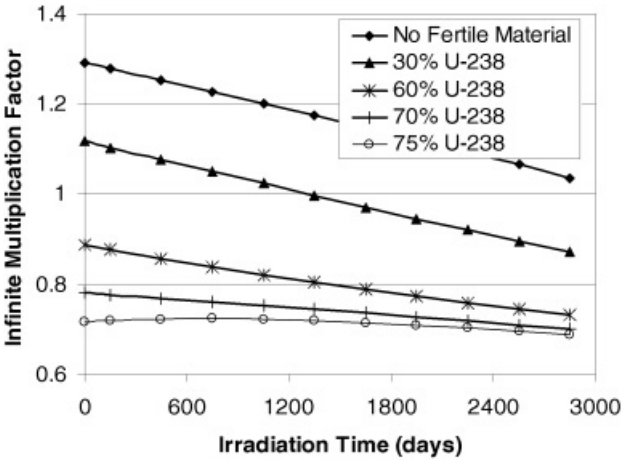


Fig. 28. Infinite lattice multiplication factor.

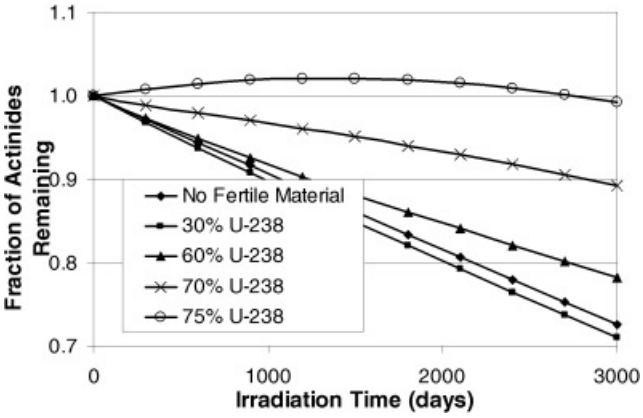


Fig. 29. Fractional burnup of nonuranium actinides.

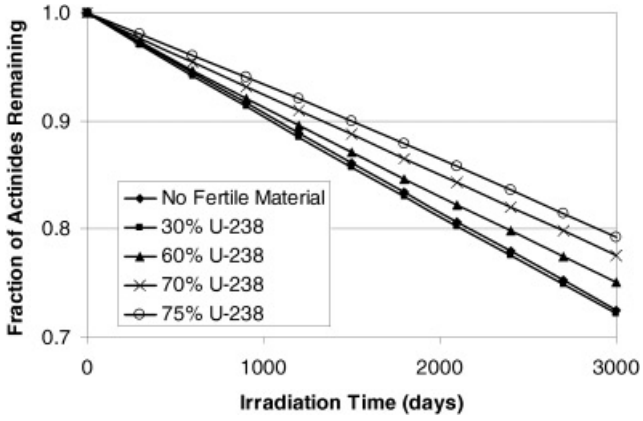


Fig. 30. Fractional burnup of TRU + $^{238}$U.

irradiation time. Since system leakage will not be significantly altered by changes in fuel composition, the trends exhibited by the value of $k_{\text{inf}}$ should be representative of trends in the $k_{eff}$ value for a whole reactor. While intuitively it seems as though any addition of fertile material would result in a reduced decrement in the multiplication factor over a given time interval, this behavior is not readily observable until a fertile concentration of nearly 70% is reached. At this concentration the infinite multiplication factor for the system is $<0.8$, which would require a fusion neutron source with more than 200 MW of fusion power.

With the addition of fertile material that is transmuted into TRU, it is no longer possible to characterize deep burn in terms of TRU burnup, as described before. Instead, the net TRU destruction, which will be defined as the percentage drop in the mass of actinides excluding uranium, will be used. This definition takes into account the reduced effectiveness of transmutation due to production of new actinides in the fertile material, but also the increased utilization of the potential energy content of the uranium. Although fertile material addition does reduce the decrement in the multiplication factor, the result is a significantly lower rate of actinide destruction as illustrated in Fig. 29.

Looking at the goal of the GCFTR-3 as resource utilization, instead of actinide destruction, suggests that the fractional burnup of the initial TRU + $^{238}$U in the fuel is a more meaningful performance measure. This quantity is plotted in Fig. 30.

The addition of fertile material to the TRU fuel results in several pros and cons in terms of the overall goals of the GCFTR as a transmutation reactor. Due to the breeding taking place in the fertile material, the rate of drop in the $k_{eff}$ is significantly lower at high fertile concentrations than with no fertile material present. This trend presents the potential for designing longer fuel cycles for neutron sources with $P_{fus} \leq 200$ MW than would be achievable without fertile admixing. Table XVII provides a comparison of design parameters for two fuel cycle lengths and two fertile admixed compositions.

Because of the large amount of fertile material that must be added in order for the benefit to be obtained, there is a large reduction in the initial fissile inventory and therefore a much lower multiplication factor for the system. In addition, there is a lower net TRU destruction rate due to the significantly lower TRU loading. These factors provide significant obstacles in the feasibility of this concept as an actinide burner, but indicate its promise for improving uranium resource utilization.

## VIII. SUMMARY AND CONCLUSIONS

The fourth in a series[3,4,7] of investigations of achieving deep burn of TRU from SNF by using it in coated TRISO particles to fuel subcritical, gas-cooled fast reactors driven by tokamak fusion neutron sources has been described. The overall study was organized into related

TABLE XVII

Steady-State Fuel Cycle Parameters with Fertile Admixing

| Parameter | A | B | C | D |
|---|---|---|---|---|
| Cycle length (days) | 600 | 600 | 1800 | 1800 |
| Fertile admixing | None | 70% $^{238}$U | None | 70% $^{238}$U |
| Five-batch residence time (yr) | 8.2 | 8.2 | 24.7 | 24.7 |
| BOC $k_{eff}$ | 0.987 | 0.590 | 0.856 | 0.577 |
| EOC $k_{eff}$ | 0.927 | 0.576 | 0.714 | 0.534 |
| BOC $P_{fus}$ (MW) | 13 | 410 | 144 | 423 |
| EOC $P_{fus}$ (MW) | 73 | 424 | 286 | 466 |
| TRU-U BOC loading (metric tons) | 37 | 37 | 37 | 37 |
| Non-$^{238}$U actinide BOC loading (metric tons) | 37 | 11.1 | 37 | 11.1 |
| TRU-U burned per year (metric tons/EFPY) | 1.12 | 1.17 | 1.09 | 1.12 |
| Non $^{238}$U actinides burned (metric tons/EFPY) | 1.12 | 0.15 | 1.09 | 0.24 |
| TRU-U burned per residence (%) | 24.9 | 25.9 | 72.4 | 74.6 |
| Non-$^{238}$U actinides burned (%) | 24.9 | 10.8 | 72.4 | 16.0 |
| SNF disposed per year (metric tons/EFPY) | 100.8 | 13.5 | 97.7 | 21.6 |
| LWR support ratio | 3 | <1 | 3 | <1 |
| Average core flux across cycle (n/cm$^2$-s) | 5.91E+14[a] | 1.04E+15 | 8.67E+14 | 1.25E+15 |
| Average fast (>0.1 MeV) flux (n/cm$^2$-s) | 2.66E+14 | 4.69E+14 | 3.90E+14 | 5.62E+14 |
| Fluence per residence time (n/cm$^2$) | 1.53E+23 | 2.70E+23 | 6.74E+23 | 9.72E+23 |
| Fast (>0.1 MeV) fluence per residence (n/cm$^2$) | 6.89E+22 | 1.22E+23 | 3.03E+23 | 4.37E+23 |

[a]Read as $5.91 \times 10^{14}$.

studies in the fuels, nuclear, thermal, neutron source, and fuel cycle areas.

Objectives of the study in the fuels area were (a) to design a TRISO particle with better probability of survival in a fast flux, (b) to choose a reference fuel pin clad material to support the deep burn mission, (c) to design the fuel fabrication system, and (d) to design a reprocessing system for TRISO fuel particles in the event that a reprocessing fuel cycle is required to achieve deep burn. The fuel pin design consisted of TRISO particles in a SiC matrix clad with ODS martensitic steel, with the TRISO particles having a reduced size TRU-oxide kernel surrounded in turn by a ZrC buffer layer, a WC layer, a SiC structural layer and an outer WC layer. Reprocessing the TRISO particle by grinding it down and then using the UREX/TRUEX process was judged feasible, though not attractive.

Objectives of the study in the nuclear design area were (a) to accommodate ports for plasma H&CD power, (b) to achieve tritium self-sufficiency, (c) to achieve a negative fuel Doppler coefficient, (d) to enhance passive safety, and (e) to simplify the shield design. The resulting core design consisted of two symmetric 160-deg semiannular core segments 1.1 m wide × 3 m high surrounding the tokamak plasma neutron source on the outboard. The core would operate with $k_{eff} \leq 0.95$, a negative Doppler coefficient and a negative coolant voiding reactivity worth. The semiannular reactor and plasma were surrounded by a 15-cm $Li_2O$-containing TBB, which in turn was surrounded by a 64.5-cm shield (steel, Ir, Cd, $B_4C$, WC, HfC).

Objectives of the study in the thermal design area were (a) to confirm the heat removal from the new fuel pins and (b) to define a design that was passively safe against a LOCA. A LOCA analysis confirmed the previously identified[3] need for an ECCS, and a passively activated, pressurized, toroidal He accumulator located either above or below the annular core segments was incorporated into the design. Fuel pin temperatures during a LOCA with ECCS were predicted to remain below the respective melting points, thus providing passive safety against the LOCA.

Objectives of the study in the fusion neutron source area were (a) to examine the possibility of extending the source strength beyond the previous[3,4] $P_{fus} \leq 200$ MW(thermal) level without changing dimensions or exceeding the present plasma physics database, (b) to confirm the feasibility of adapting the ITER divertor design from water to He cooling, (c) to adapt the ITER H&CD system, and (d) to modify the designs of the superconducting magnet systems to remain within the ITER stress limits when the fusion power was increased. It was judged feasible to extend the fusion neutron source strength up to 500 MW(thermal) by a 20% increase in plasma current, without changing dimensions or magnetic field, without exceeding ITER magnet system stress limits, and without significantly exceeding the present ITER physics database. Detailed heat removal calculations indicated that the ITER divertor adapted to He coolant could handle surface heat loads up to at least 2 MW/m$^2$ without excessive pumping power requirements. An LH electromagnetic H&CD system to

TABLE A.I

Materials Composition of FTWR and GCFTR

| Component | FTWR | GCFTR |
|---|---|---|
| Reactor | | |
| Fuel | TRU-Zr metal in Zr matrix | TRU-oxide TRISO, SiC matrix |
| Clad/structure | FeS/FeS | ODS/ODS |
| Coolant | LiPb | He |
| Tritium breeder | LiPb | $Li_2O$ |
| Reflector | FeS, LiPb | ODS, He, $Li_2O$ |
| Shield | FeS, LiPb, $B_4C$, $ZrD_2$, W | ODS, HfC, Ir, Cd, WC, $B_4C$, He |
| Magnets | NbSn, NbTi/He (OFHC/$LN_2$) | NbSn/He |
| First wall | Be-coated FeS, LiPb | Be-coated ODS, He |
| Divertor | W-tiles on Cu-CuCrZr, LiPb | W-tiles on Cu-CuCrZr, He |

deliver up to 100 MW(thermal) heating power and drive 7.5 MA of plasma current was adapted from the ITER design.

Objectives of the study in the fuel cycle area were (a) to investigate deep burn fuel cycles that would achieve very high burnup of TRU-oxide fuels and (b) to investigate high uranium utilization fuel cycles that would extract very high fractions of the potentially available energy in TRU-$^{238}$U-oxide fuels. It appears possible to achieve >90% burnup of TRU-oxide fuel with near-term fusion neutron sources producing up to 400 MW(thermal), without reprocessing, provided that the fuel can survive the associated radiation damage. It also appears possible to achieve similarly high burnup in cores loaded with 70% $^{238}$U–30% TRU fuel without reprocessing, using fusion neutron sources producing up to 500 MW(thermal), again providing that the fuel can survive the radiation damage. The composition used for the TRU fuel is given in Appendix B.

Thus, the overall conclusion of this study is that it is possible to design a passively safe, subcritical GCFTR, with a 400 to 500 MW(thermal) tokamak fusion neutron source only slightly exceeding the present ITER design database, which can achieve ≥90% burnup of the TRU-oxide or 70% $^{238}$U–30% TRU-oxide fuel in TRISO particles without the need to reprocess, if the fuel can withstand the radiation damage. If the fuel can not withstand the fast neutron fluence of $4 \times 10^{23}$ n/cm$^2$ associated with 90% burnup, then it will be necessary to reprocess the fuel to achieve 90% burnup, and a less intense neutron source will suffice.

## APPENDIX A

## FTWR AND GCFTR PHYSICAL CHARACTERISTICS

A summary of the physical characteristics of the two series of subcritical, fast transmutation reactor driven by a tokamak fusion neutron source, concepts that have been developed in the Georgia Tech studies, are given in this appendix. The FTWR concept[1,2,5,6] is based on the Integral Fast Reactor with metal TRU-oxide fuel and lead-lithium euctectic cooling. The GCFTR concept,[3,4,7] the latest manifestation of which is the subject of this paper, is based on the gas-cooled fast reactor with coated TRISO TRU-oxide fuel and helium coolant. The materials composition and core/fuel parameters are given in Tables A.I and A.II, respectively.

The tokamak plasma neutron source parameters are compared in Table A.III to those that are confidently expected to be achieved in ITER (initial operation 2016–2019) to make the point that successful operation of ITER will serve as a prototype for the fusion neutron source needed for the FTWR and GCFTR-type subcritical transmutation reactors. The achievement of high current drive efficiency and bootstrap current need for semicontinuous operation to achieve high availability is a major focus of current magnetic fusion research and may also be achieved in ITER.

TABLE A.II

Core and Fuel Assembly Parameters

| | FTWR | GCFTR |
|---|---|---|
| Core inner radius (cm) | 500 | 485 |
| Core width (cm) | 40 | 112 |
| Core height (cm) | 228 | 300 |
| Pin diameter (cm) | 0.635 | 1.526 |
| Pins per assembly | 217 | 384 |
| Assembly flat-to-flat (cm) | 16.1 | 36.6 |
| Assembly length (cm) | 228 | 300 |
| Assemblies in core | 470 | 245 |
| Core cool flow (kg/s) | 51 630 | 3280 |
| Coolant $T_{in}/T_{out}$ (K) | 548/848 | 553/767 |
| Materials (vol%) | | |
| Fuel | 20 | 60 |
| Structure | 10 | 10 |
| Coolant | 70 | 30 |

TABLE A.III

Tokamak Neutron Source Parameters for FTWR and GCFTR Transmutation Reactors*

| Parameter | FTWR[a] | FTWR-SC[b] | FTWR-AT[c] | GCFTR[d] | GCFTR-2[e] | GCFTR-3 | ITER[f] |
|---|---|---|---|---|---|---|---|
| Max. fusion power, $P_{fus}$ (MW) | 150 | 225 | 500 | 180 | 180 | 500 | 410 |
| Max. neutron source, $S_{fus}$ ($10^{19}$/s) | 5.3 | 8.0 | 17.6 | 7.1 | 7.1 | 17.6 | 14.4 |
| Major radius, $R$ (m) | 3.1 | 4.5 | 3.9 | 4.2 | 3.7 | 3.7 | 6.2 |
| Plasma current, $I$ (MA) | 7.0 | 6.0 | 8.0 | 7.2 | 8.3 | 10.0 | 15.0 |
| Magnetic field, $B$ (T) | 6.1 | 7.5 | 5.7 | 6.3 | 5.7 | 5.9 | 5.3 |
| Normalized beta, $\beta_N$ (%) | 2.5 | 2.5 | 4.0 | 2.0 | 2.0 | 2.85 | 1.8 |
| Plasma power mult., $Q_p$[g] | 2.0 | 2.0 | 4.0 | 2.9 | 3.1 | 5.1 | 10 |
| Current drive efficiency $\gamma_{cd}$ ($10^{-20}$ A/W m$^2$) | 0.37 | 0.23 | 0.04 | 0.5 | 0.61 | 0.58 | |
| Bootstrap current fraction, $f_{bs}$ | 0.40 | 0.50 | ≥0.90 | 0.35 | 0.31 | 0.26 | |
| FW[h] neutron flux, $\Gamma_n$ (MW/m$^2$) | 0.8 | 0.8 | 1.7 | 0.9 | 0.6 | 1.8 | 0.5 |
| FW heat flux, $q_{fw}$ (MW/m$^2$) | 0.34 | 0.29 | 0.5 | 0.23 | 0.23 | 0.65 | 0.15 |

*Calculated on the basis of the physics and engineering constraints described in Ref. 45. All superconducting magnets except FTWR copper magnets. All based on ITER physics except AT based on advanced tokamak physics.
[a]Reference 1.
[b]Reference 2.
[c]Reference 64.
[d]Reference 4.
[e]Reference 3.
[f]Reference 8.
[g]$Q_P = P_{fus}/P_{heat}$.
[h]FW = first wall surrounding plasma.

## APPENDIX B

## TRU FUEL COMPOSITION

The composition used for the TRU fuel is given in Table B.I.

TABLE B.I

TRU Fuel Composition

| Isotope | TRU Fuel Composition (g/100 g initial fresh fuel) | | | | |
|---|---|---|---|---|---|
| | Fresh Fuel | End of 600-Day Cycle | End of 1200-Day Cycle | End of 1800-Day Cycle | End of 2400-Day Cycle |
| $^{232}$U | 2.9374E−10[a] | 7.6258E−06 | 7.9727E−06 | 3.1140E−08 | 4.2462E−08 |
| $^{233}$U | 2.1782E−09 | 6.4981E−06 | 7.7866E−06 | 4.7018E−08 | 5.3987E−08 |
| $^{234}$U | 7.0823E−05 | 1.6197E−01 | 2.7245E−01 | 2.2525E−03 | 2.1903E−03 |
| $^{235}$U | 3.1567E−03 | 2.8065E−02 | 9.2736E−02 | 1.8648E−03 | 4.6303E−03 |
| $^{236}$U | 1.4454E−03 | 2.1298E−02 | 4.9835E−02 | 2.7500E−03 | 7.6204E−03 |
| $^{238}$U | 5.2869E−03 | 4.0902E−03 | 2.5503E−03 | 1.9205E+00 | 2.0404E−04 |
| $^{237}$NP | 4.4254E+00 | 2.0181E+00 | 5.0987E−01 | 1.7953E−03 | 6.4013E−03 |
| $^{238}$Pu | 1.2544E+00 | 4.7519E+00 | 4.4178E+00 | 5.9766E−02 | 1.2508E−01 |
| $^{239}$Pu | 5.4236E+01 | 2.4735E+01 | 6.6034E+00 | 6.5764E−01 | 5.1329E−02 |
| $^{240}$Pu | 2.1324E+01 | 2.4904E+01 | 1.9528E+01 | 8.8424E−01 | 2.5827E−02 |
| $^{241}$Pu | 3.8709E+00 | 4.3984E+00 | 5.1619E+00 | 3.4820E−01 | 7.1294E−02 |
| $^{242}$Pu | 4.6369E+00 | 5.1353E+00 | 5.6353E+00 | 3.7475E−01 | 9.9634E−02 |
| $^{244}$Pu | 1.5733E−04 | 1.3814E−04 | 1.4298E−04 | 4.0823E−05 | 3.4151E−04 |
| $^{241}$Am | 9.1002E+00 | 5.0839E+00 | 2.2882E+00 | 4.3264E−02 | 8.4291E−03 |
| $^{242m}$Am | 6.5878E−03 | 3.4440E−01 | 1.8472E−01 | 2.9676E−03 | 8.1834E−04 |
| $^{243}$Am | 1.0087E+00 | 1.2437E+00 | 1.5322E+00 | 1.5396E−01 | 1.3446E−01 |
| $^{242}$Cm | 9.2192E−06 | 2.2290E−01 | 1.7667E−01 | 7.6960E−03 | 4.1102E−03 |
| $^{243}$Cm | 9.3018E−04 | 4.9125E−02 | 5.6601E−02 | 1.9505E−03 | 7.9947E−04 |
| $^{244}$Cm | 6.0349E−02 | 5.7713E−01 | 1.2764E+00 | 2.0166E−01 | 6.1496E−01 |
| $^{245}$Cm | 6.5177E−02 | 1.1134E−01 | 3.5943E−01 | 1.0069E−01 | 4.9193E−01 |
| $^{246}$Cm | 5.1570E−04 | 8.6340E−03 | 4.7923E−02 | 4.5317E−02 | 5.7660E−01 |
| $^{247}$Cm | 5.2013E−06 | 5.0499E−04 | 4.9527E−03 | 1.1335E−02 | 1.4519E−01 |

[a]Read as $2.9374 \times 10^{-10}$.

## REFERENCES


1. W. M. STACEY et al., "A Fusion Transmutation of Waste Reactor," *Fusion Sci. Technol.*, **41**, 116 (2002).

2. A. N. MAUER, W. M. STACEY, J. MANDREKAS, and E. A. HOFFMAN, "A Superconducting Tokamak Fusion Transmutation of Waste Reactor," *Fusion Sci. Technol.*, **45**, 55 (2004).

3. W. M. STACEY et al., "A Subcritical, Helium Cooled, Fast Reactor for the Transmutation of Spent Nuclear Fuel," *Nucl. Technol.*, **156**, 99 (2006).

4. W. M. STACEY et al., "A Subcritical, Gas-Cooled Fast Transmutation Reactor with a Fusion Neutron Source," *Nucl. Technol.*, **150**, 162 (2005).

5. W. M. STACEY, J. MANDREKAS, and E. A. HOFFMAN, "Sub-Critical Transmutation Reactors with Tokamak Fusion Neutron Sources," *Fusion Sci. Technol.*, **47**, 1210 (2005).

6. E. A. HOFFMAN and W. M. STACEY, "Comparative Fuel Cycle Analysis of Critical and Subcritical Fast Reactor Transmutation Systems," *Nucl. Technol.*, **144**, 83 (2003).

7. J. W. MADDOX and W. M. STACEY, "Fuel Cycle Analysis of a Subcritical, Fast, He-Cooled Transmutation Reactor with a Fusion Neutron Source," *Nucl. Technol.* (to be published).

8. ITER Web site; available on the Internet at http://iter.org.

9. LONG et al., "Fabrication of ORNL Fuel Irradiated in the Peachbottom Reactor and Post-Irradiation Examination of the Recycle Test Elements 7 and 4," Oak Ridge National Laboratory (Oct. 1974).

10. D. A. PETTI et al., "Key Differences in the Fabrication, Irradiation and High Temperature Accident Testing of U. S. and German TRISO-Coated Particle Fuel, and Their Implications on Fuel Performance," *Nucl. Eng. Des.*, **222**, 281 (2003).

11. B. KADOMTSEV et al., "USSR Contribution to the Phase IIA INTOR Workshop," Vol. 2, p. VIII-64 (1982).

12. M. SAWAN, University of Wisconsin, Personal Communication (2004).

13. "Fuel Performance and Fission Product Behavior in Gas Cooled Reactors," IAEA-TECDOC-978, International Atomic Energy Agency (1997).

14. W. VAN ROOJEN, "Improving Fuel Cycle Design and Safety Characteristics of a Gas Cooled Reactor," PhD Thesis, Delft University of Technology (2006).

15. K. MILLER et al. "Consideration of the Effects of Partial Debonding of the IPyC and Particle Asphericity on TRISO-Coated Fuel Behavior," *J. Nuc. Mater.*, **334**, 79 (2004).

16. I. C. GAULD, O. W. HERMANN, and R. M. WESTFALL, "ORIGEN-S: SCALE System Module to Calculate Fuel Depletion, Actinide Transmutation, Fission Product Buildup and Decay, and Associated Radiation Source Terms," NUREG/CR-0200, Revision 7, Volume II, Section F7 (ORNL/NUREG/CSD-2/V2/R7) U.S. Nuclear Regulatory Commission, Oak Ridge National Laboratory (2004).

17. M. ZHOU, Georgia Institute of Technology, Personal Communication (2006).

18. J. T. BUSBY, Oak Ridge National Laboratory, Personal Communication (2006).

19. S. T. NOZAWA et al., "Determining the Shear Properties of the PyC/SiC Interface for a Model TRISO Fuel," *J. Nucl. Mater.*, **350**, 182 (2006).

20. T. YOSHITAKE et al., "Ring-Tensile Properties of Irradiated Oxide Dispersion Strengthened Ferritic/Martensitic Steel Claddings," *J. Nucl. Mater.*, **344**, 329 (2004).

21. S. UKAI and M. FUJIWARA, "Perspective of ODS Alloys Application in Nuclear Environments," *J. Nucl. Mater.*, **307**, 749 (2004).

22. S. UKAI et al., "R&D of Oxide Dispersion Strengthened Ferritic Martensitic Steels for FBR," *J. Nucl. Mater.*, **258**, 1745 (1998).

23. S. ZINKLE, "Advanced Materials for Fusion Technology," presented at 23rd Symp. Fusion Technology, Venice, Italy, September 20–24, 2004.

24. R. JONES, "$SiC_f$/SiC Composites for Advanced Nuclear Applications," *Ceramic Engineering and Science Proc., Vol. 24: Proc. 27th Annual Conf. and Exposition Advanced Ceramics and Composites*, Cocoa Beach, Florida, January 26–31, 2003, p. 261, American Ceramic Society (2003).

25. "NIST Property Data Summary for Silicon Carbid (SiC)," National Institute of Standards and Technology; available on the Internet at http://www.ceramics.nist.gov/srd/summary/ftgsic.htm (Feb. 2001).

26. J. BOTTCHER, S. UKAI, and M. INOUE, "ODS Steel Clad Mox Fuel-Pin Fabrication and Irradiation Performance in EBR-II," *Nucl. Technol.*, **138**, 238 (2002).

27. H. BAIRIOT and G. VANHELLEMONT, "Production of Thorium- and Plutonium-Diluted Sol-Gel Particles," *Sol-Gel Processes for Ceramic Nuclear Fuels, Proc. Panel on Sol-Gel Processes for Ceramic Nuclear Fuels*, Vienna, Austria, May 6–10, 1968, International Atomic Energy Agency (1968).

28. R. G. WYMER, "Laboratory and Engineering Studies of Sol-Gel Processes at Oak Ridge National Laboratory," *Sol-Gel Processes for Ceramic Nuclear Fuels, Proc. Panel on Sol-Gel Processes for Ceramic Nuclear Fuels*, Vienna, Austria, May 6–10, 1968, International Atomic Energy Agency (1968).

29. W. J. LACKEY and T. L. STARR, "Fabrication of Fiber Reinforced Ceramic Composites by Chemical Vapor Infiltration: Processing, Structure and Properties," *Fiber Reinforced Ceramic Composites*, K. S. MAZDIYASNI, Ed., Noyes Publications, Park Ridge, New Jersey (1990).

30. D. TEDDER and R. HOROWITZ, "Concepts in Waste Management: Decontamination of Plutonium-Bearing Mixed Wastes with Efficient Water and Acid Recycle," *Sep. Sci. Technol.*, **38**, 12 (2003).

31. D. W. TEDDER and E. P. HOROWITZ, "Efficient Strategies for Partitioning Actinides from Alkaline Wastes," *Ind. Engr. Chem. Res.*, **44**, *3*, 606 (2005).

32. T. TAN et al., "Simulation and Analysis for Melt Casting A Metallic Fuel Pin Incorporating Volatile Actinides," *Proc. ASME Int. Mechanical Engineering Congress and Exposition*, Washington, D.C., November 16–21, 2003, American Society of Mechanical Engineers (2003).

33. "Actinide Separation Chemistry in Nuclear Waste Streams and Materials," NEA/NSC/DOC(97)19, Organization for Economic Cooperation and Development/Nuclear Energy Agency (1997).

34. E. ZIMMER and C. GANGULY, "Reprocessing and Refabrication of Thorium-Based Fuels," Institut für chemische Technologie der nuklearen Entsorgung, Kernforschungsanlage Jülich GmbH; available on the Internet at http://www.iaea.org/inis/aws/fnss/fulltext/0412_8.pdf (2005).

35. G. VANDEGRIFT et al., "Lab-Scale Demonstration of the UREX+ Process," presented at Waste Management Conference, Tucson, Arizona, February 29–March 4, 2004.

36. J. LAW et al., "Development and Demonstration of Solvent Extraction Processes for the Separation of Radionuclides from Acidic Radioactive Waste" *Waste Management*, **19**, 27 (1999).

37. M. OZAWA et al., "A New Reprocessing System Composed of PUREX and TRUEX Processes for Total Separation of Long-Lived Radionuclides," *Proc. Fifth OECD/NEA Information Exchange Meeting on Actinide and Fission Product Partitioning and Transmutation*, Mol, Belgium; November 25–27, 1998, SCK-CEN (1998).

38. C. DE OLIVEIRA and A. GODDARD, "EVENT—A Multidimensional Finite Element-Spherical Harmonics Radiation Transport Code," *Proc. Int. Seminar 3-D Deterministic Radiation Transport Codes*, Paris, France, December 2–3, 1996, Organization for Economic Cooperation and Development (1996).

39. "MCNP—A General Monte Carlo N-Particle Transport Code, Version 5," J. F. BRIESMEISTER, Ed., Los Alamos National Laboratory (2003).

40. "KENO V.a: An Improved Monte Carlo Criticality Program," NUREG/CR-0200, Rev. 7, Vol. II, Section F11, ORNL/NUREG/CSD-2/R7, U.S. Nuclear Regulatory Commission (2004).

41. TRANSX 2"; available on the Internet at http://t2.lanl.gov/codes/html.

42. W. M. STACEY, *Nuclear Reactor Physics*, Chap. 2, Wiley-Interscience, New York (2001).

43. W. M. STACEY, *Fusion*, Chap. 10, Wiley-Interscience, New York (1984).

44. M. KAMBE and M. UOTANI, "Design and Development of Fast Breeder Reactor Passive Reactivity Control Systems: LEM and LIM," *Nucl. Technol.*, **122**, 179 (1998).

45. M. S. KAZIMI and N. E. TODREAS, *Nuclear Systems I: Thermal Hydraulics Fundamentals*, pp. 295–338, Hemisphere Publishing Corporation, New York (1990).

46. M. J. MORAN and H. N. SHAPIRO, *Fundamentals of Engineering Thermodynamics*, 4th ed., pp. 441–467, John Wiley & Sons, Inc, New York (2000).

47. E. TEUGHERT, K. HAAS, A. VAN HEEK, and P. KASTEN, "Distribution of the Decay Heat in Various Modular HTRs and Influence on Peak Fuel Temperatures," presented at Energy Conversion Engineering Conference, Philadelphia, Pennsylvania, August 10–14, 1987.

48. M. S. KAZIMI and N. E. TODREAS, *Nuclear Systems I: Thermal Hydraulics Fundamentals*, pp. 16–17, 417, 684–685, Hemisphere Publishing Corporation, New York (1990).

49. W. M. STACEY, *Fusion Plasma Physics*, Chap. 19, Wiley-VCH Verlag GmbH & Co. KGaA, Weinheim, Germany (2005).

50. J. SCHLOSSER et al., *Nucl. Fusion*, **45**, 512 (2005).

51. "ITER Technical Basis," Section 2.4, "Divertor," International Atomic Energy Agency (2001).

52. "Computational Fluid Dynamics," Fluent/Gambit, Version 6.1.22/s.1.2, Fluent Inc. (2004).

53. C. B. BAXI and C. P. C. WONG, "Review of Helium Cooling for Fusion Reactor Applications," *Fusion Eng. Des.*, **51–52**, 319 (2000).

54. F. P. INCROPERA and D. P. DeWITT, *Fundamentals of Heat and Mass Transfer*, 5th ed., Chap. 8, John Wiley & Sons, Hoboken, New Jersey (2002).

55. B. R. MUNSON, D. F. YOUNG, and T. H. OKIISHI, *Fundamentals of Fluid Mechanics*, 4th ed., Chap. 8, John Wiley & Sons, Hoboken, New Jersey (2002).

56. ITER Technical Basis, Chap. 2.5 Additional Heating and Current Drive, G A0 FDR 101-07-13 R1.0 (2001).

57. "Technical Parameters" Web Site http://www.iter.org/index.htm.

58. R. D. STAMBAUGH, "Future of Tokamak Facilities with a Burning Plasma Experiment," presentation to National Academies Burning Plasma Assessment Committee, 008-03/RDS/RS, January 18, 2003.

59. Y. SAKAMOTO et al., "Stationary High Confinement Plasmas with Large Bootstrap Current Fraction in JT-60U," EX/4-3.

60. ITER Technical Basis, Chapter 2.1 Magnets, G A0 FDR 1 01-07-13 R1.0 (2001).

61. M. HUGUET, "Key Engineering Features of the ITER-FEAT Magnet System and Implications for the R&D Programme," *Nucl. Fusion*, **41**, 645 (2001).

62. "Triton: A Two-Dimensional Depletion Sequence for Characterization of Spent Nuclear Fuel," NUREG/CR-200, Rev. 7, Vol. I Section T1, ORNL/NUREG/CSD-2/R7 (2004).

63. N. F. LANDERS, L. M. PETRIE, and D. F. HOLLENBACH, "CSAS: Control Module for Enhanced Criticality Safety Analysis Sequences," NUREG/CR-200, Rev. 7, Vol. 1 Section C4, ORNL/NUREG/CSD-2/V1/R7.

64. J. MANDREKAS, L. A. COTTTRILL, G. C. HAHN, and W. M. STACEY, "An Advanced Tokamak Neutron Source for a Fusion Transmutation of Waste Reactor," Georgia Tech report GTFR-167 (2003).